FAA-RD-75-91

Project Report
ATC-50

Impact of Obstacle Shadows on Monopulse Azimuth Estimate

A. Spiridon

17 July 1975

Lincoln Laboratory
MASSACHUSETTS INSTITUTE OF TECHNOLOGY
LEXINGTON, MASSACHUSETTS

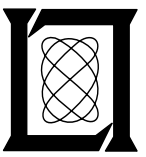

Prepared for the Federal Aviation Administration,
Washington, D.C. 20591.

This document is available to the public through
the National Technical Information Service,
Springfield, VA 22161

Technical Report Documentation Page

1. Report No.	2. Government Accession No.	3. Recipient's Catalog No.
FAA-RD-75-91		

4. Title and Subtitle	5. Report Date
Impact of Obstacle Shadows on Monopulse Azimuth Estimate	17 July 1975
	6. Performing Organization Code

7. Author(s)	8. Performing Organization Report No.
A. Spiridon	ATC-50

9. Performing Organization Name and Address	10. Work Unit No. (TRAIS) 45364
Massachusetts Institute of Technology Lincoln Laboratory P.O. Box 73 Lexington, Massachusetts 02173	Project No. 034-241-012
	11. Contract or Grant No. IAG DOT-FA72-WAI-261
	13. Type of Report and Period Covered Project Report
12. Sponsoring Agency Name and Address Department of Transportation Federal Aviation Administration Systems Research and Development Service Washington, D.C. 20591	14. Sponsoring Agency Code

15. Supplementary Notes

The work reported in this document was performed at Lincoln Laboratory, a center for research operated by Massachusetts Institute of Technology under Air Force Contract F19628-76-C-0002.

16. Abstract

Obstacle shadows, within view of a sensor using monopulse azimuth estimate, cause an error in the azimuth estimate. This report discusses the azimuth error as a function of obstacle dimension and position, and the sensor antenna illumination.

17. Key Words	18. Distribution Statement
Monopulse azimuth error Obstacle shadow DABS performance	Document is available to the public through the National Technical Information Service, Springfield, Virginia 22151.

19. Security Classif. (of this report)	20. Security Classif. (of this page)	21. No. of Pages	
Unclassified	Unclassified	60	

TABLE OF CONTENTS

ILLUSTRATIONS

ILLUSTRATIONS (cont.)

ILLUSTRATIONS (cont.)

TABLES

IMPACT OF OBSTACLE SHADOWS ON MONOPULSE AZIMUTH ESTIMATE

1.0 INTRODUCTION

The Discrete Address Beacon System (DABS) uses a monopulse receiver-processor that makes an estimate of the off-boresight angle for each received pulse of the ATCRBS or DABS reply [Ref. 1] and then combines the individual measurements to provide a single estimate for the whole reply. This report deals with the obstacle shadow azimuth error (SAE), both in terms of its impact on sensor coverage and the detailed character of its spatial distribution. Interest in SAE was motivated by the attempt to explain the anomalous performance of aircraft tracks close to obstacles that project above the horizon [Ref. 2].

Shadow azimuth errors could be a problem for a sensor at a site with tall obstacles in the skyline. An error in azimuth is introduced into the target positions that are close in azimuth to tall obstacles. The Boston skyline, as seen from Logan Airport, represents such an example when the total azimuth extent of obstacles, with an elevation of one degree or higher, is 15.5 degrees. Figures 1-1a, 1-1b, and 1-1c are part of the Boston skyline; the tall obstacles are high rise buildings and smokestacks.

The shadow azimuth error, caused by actual obstacles, is illustrated by a smokestack in Fig. 1-2 (Hanscom Field), and by a high-rise building (Prudential) in Fig. 1-3. Figures 1-4 and 1-5 are photographs of the obstacles as seen from the sensor at which the azimuth error is computed. It is observed that the magnitude and spatial distribution of SAE are affected by the obstacle position with respect to the sensor and its dimensions. The high-rise building produces an error of $\pm$ 0.8 degree; and its SAE is practically confined to an azimuth wedge of 0.5 degree, while the smokestack SAE assumes values of $\pm$ 0.3 degree and is practically confined to an azimuth wedge of 6.4 degrees.

ATC-50 (1-1a)

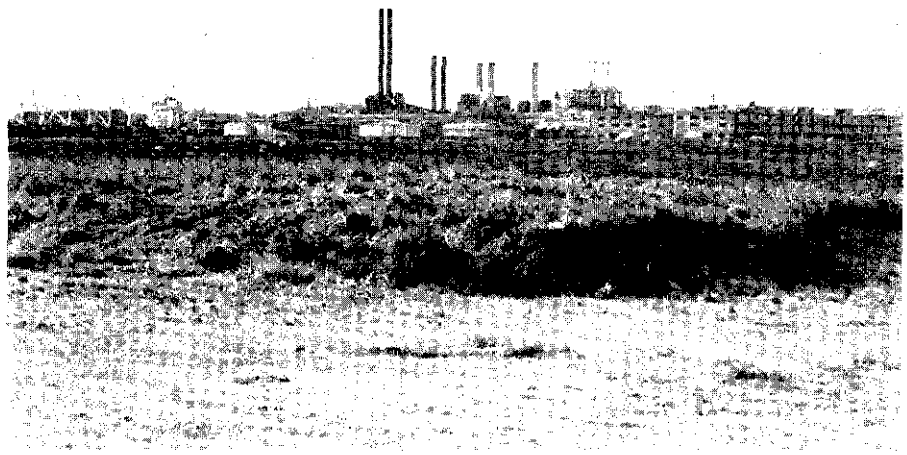

Fig. 1-1(a). Smokestacks (part of Boston skyline as seen from Logan Internation Airport.

ATC-50 (1-1b)

Fig. 1-1(b). Highrise buildings (part of Boston skyline as seen from Logan Airport).

ATC-50 (1-1c)

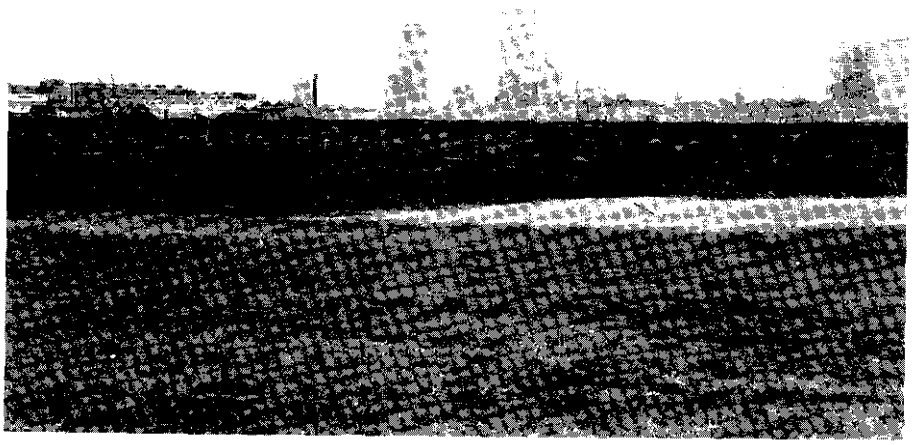

1-1(c). Highrise buildings (a second view of part of Boston skyline as seen from Logan Airport).

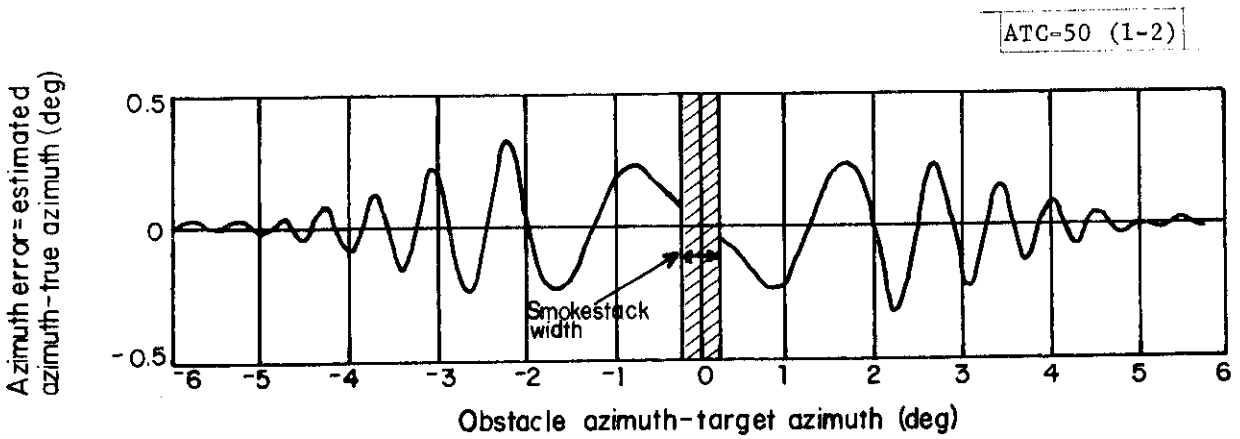

Fig. 1-2. Azimuth estimation error vs obstacle position. Obstacle, which corresponds to Hanscom Field smokestack as seen from DABSEF, is 10 feet wide and at a 1500-foot range (λ = 1 ft).

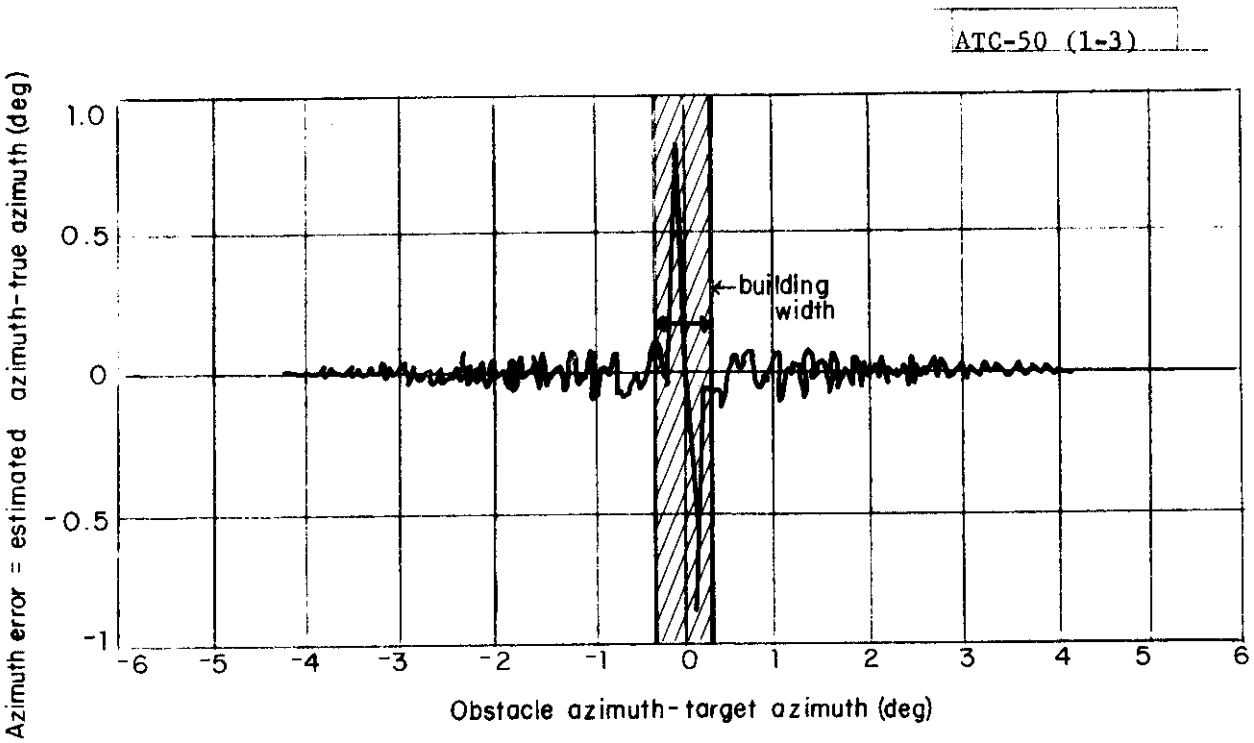

Fig. 1-3. Azimuth estimation error vs obstacle position. Obstacle, which corresponds to Prudential building as seen from Logan Airport, is 200 feet wide and at a 20, 000-ft range. (λ = 1 ft).

ATC-50 (1-4)

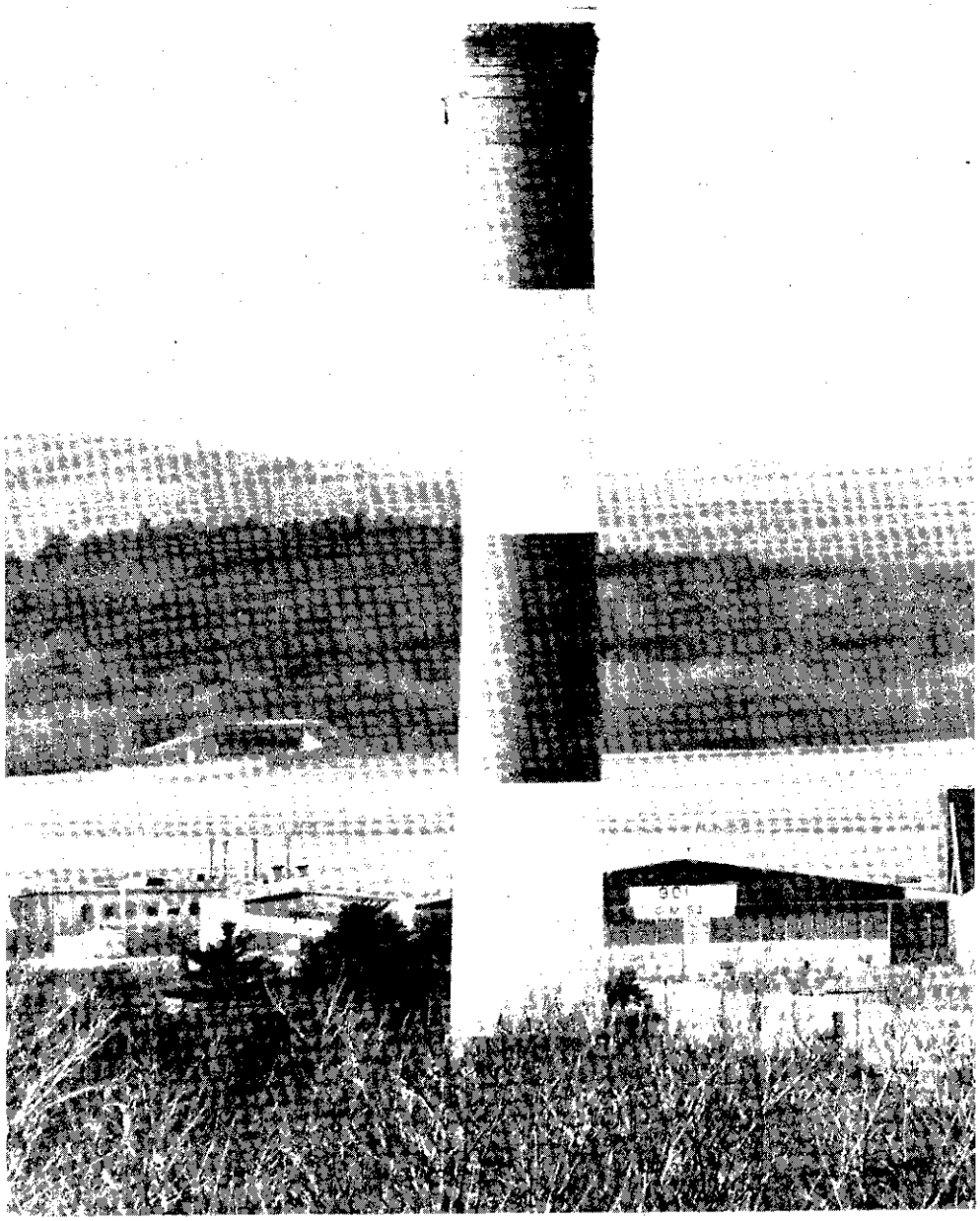

Fig. 1-4. Blow-up of the Hanscom smokestack as seen from DABSEF.

ATC-50 (1-5)

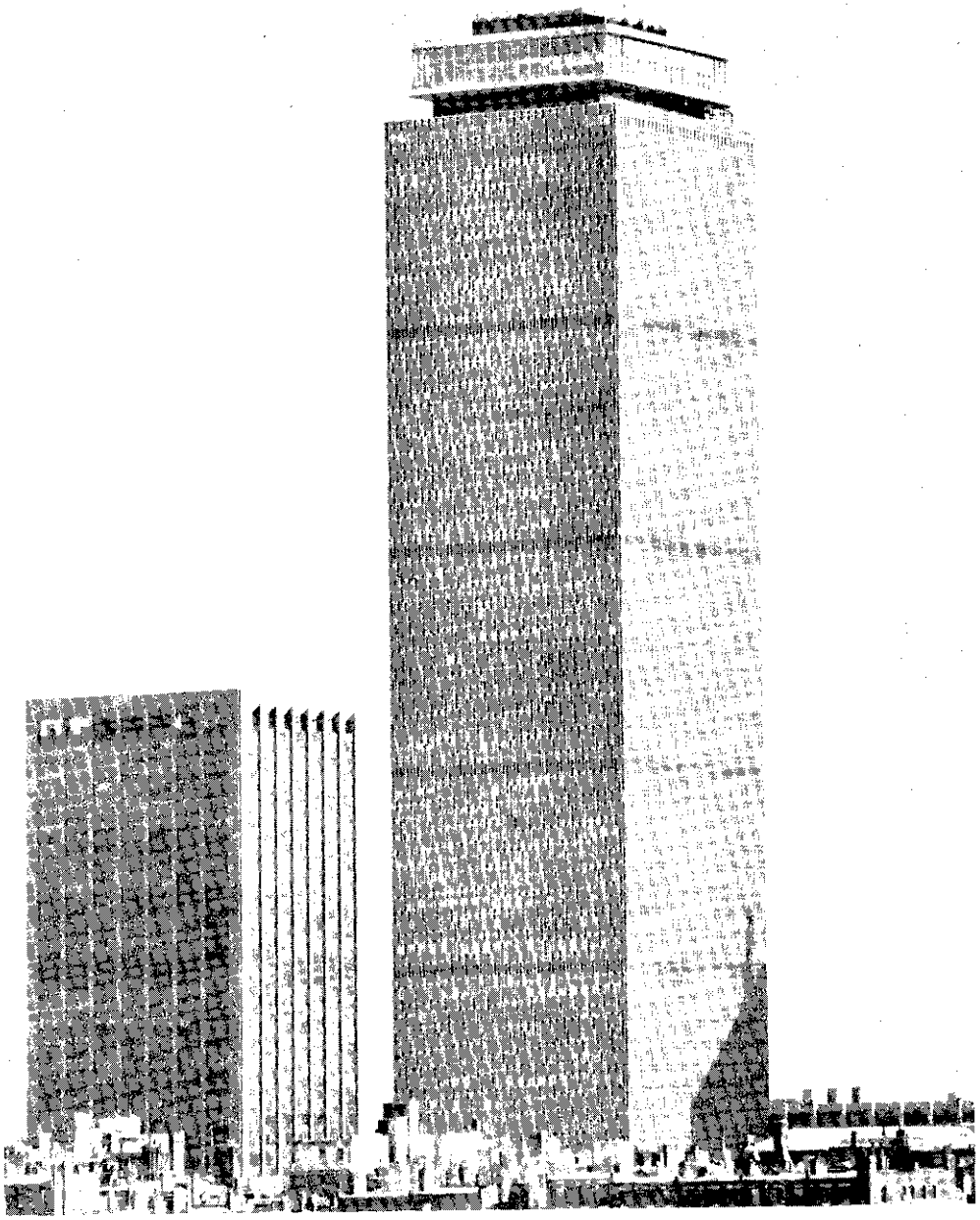

Fig. 1-5. Blow-up of Prudential building as seen from Logan Airport.

2.0 ENVIRONMENT PARAMETERS CRITICAL TO AZIMUTH ERROR

2.1 Definition of Parameters

The azimuth error, hereinafter used to denote the error in the azimuth estimate caused by the shadow of obstacles, is affected by the dimensions of the obstacle as well as the positions of both the aircraft and the obstacle relative to the antenna. Dimensions are expressed in terms of wavelength, λ: DABS uses a wavelength of approximately 1 ft. The parameters used to discuss the results are illustrated in Fig. 2-1 and explicitly defined as follows:

(a) The azimuth error (deg) is the reported bearing of the aircraft relative to its actual bearing (clockwise angles are positive).

(b) The obstacle angle (deg) is the obstacle bearing relative to the aircraft (clockwise angles are positive).

(c) The obstacle width (λ) is the cross-range width of the obstacle.

(d) The range of the obstacle (λ) is the range of the obstacle shadowing the aircraft from the sensor.

(e) The range of the aircraft (λ) is the range from the sensor of the aircraft whose azimuth is estimated.

(f) The bearing of the aircraft (deg) is the off-boresight angle of the aircraft (positive when the aircraft is to the right of the boresight).

2.2 Nominal Operating Conditions

The results of the report are for nominal operating conditions unless specifically noted. The nominal conditions are:

(a) The obstacle shadowing the aircraft is isolated and tall so that the line joining the sensor to the aircraft is much below the top of the obstacle (see Fig. 2-1). Reflections from the obstacle are not examined in this report.

(b) The shadow azimuth error is for an aircraft at boresight; it will be shown in Chapter 5 that this gives an average error if several interrogations were addressed to the aircraft at equal increments of off-boresight angle.

(c) A Lincoln Laboratory DABSEF planar array antenna that has a ~3 deg beamwidth is used to estimate the aircraft azimuth. The illumination pattern is included in Appendix A.

(d) The aircraft range is much larger than the obstacle range: most obstacles that significantly project above the horizon are within a few miles from the sensor.

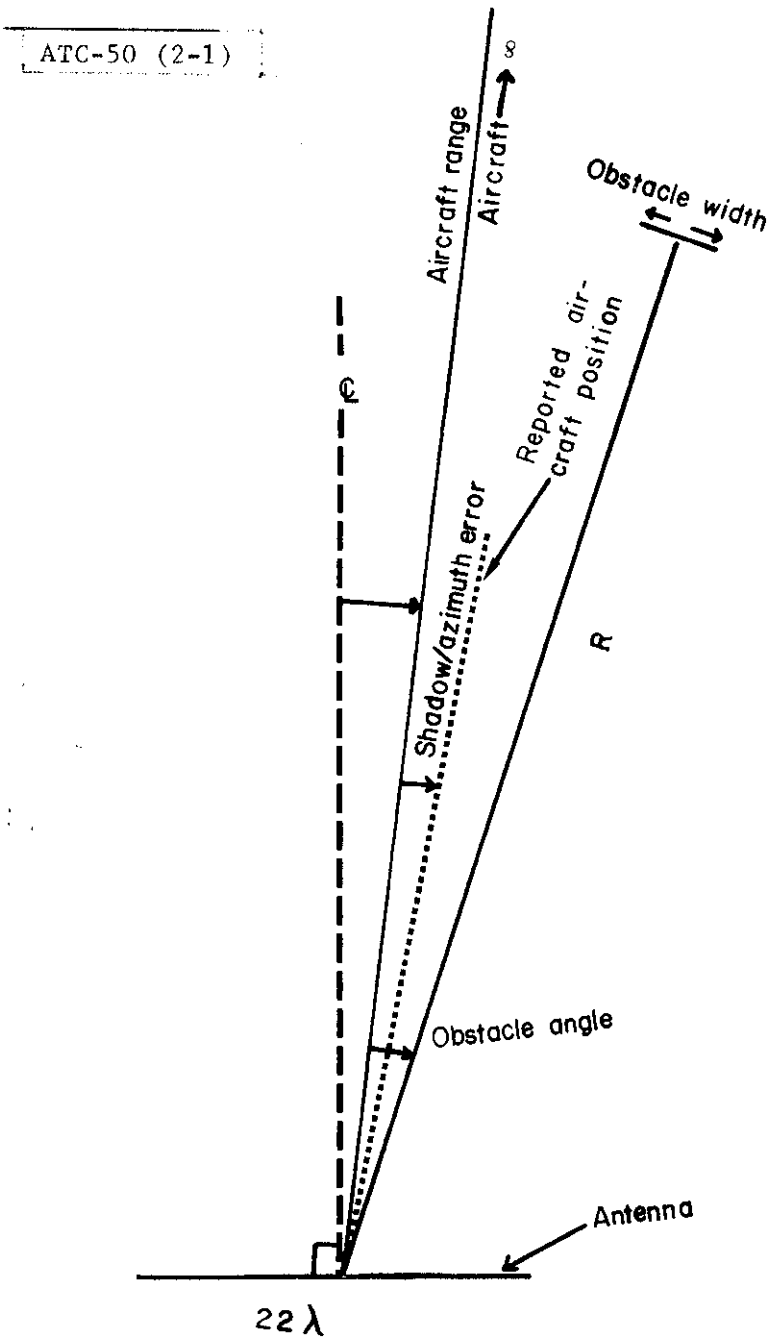

Fig. 2-1. Parameters used in study of shadow azimuth error.

The azimuth error was calculated using the far field gain of the antenna's individual elements and Fourier optics to compute the field at the surface of the antenna. Appendix A gives details of the computational procedure.

3.0 IMPACT OF OBSTACLE POSITIONS AND DIMENSIONS ON AZIMUTH ERROR

It is important to determine which obstacles produce significant azimuth error and the spatial extent of this error. This is accomplished on the basis of key features of the azimuth error:

- Maximum azimuth error (deg) is the peak value of the shadow azimuth error.
- Angle of maximum azimuth error (deg) is the azimuth angle off the obstacle center where the maximum azimuth error occurs.
- Error wedge (deg) is the narrow azimuth wedge centered at the obstacle that confines shadow azimuth error values greater than 0.2 degree.

The value of the key features for the Hanscom Field smokestack are:

Maximum azimuth error = 0.35 deg
Angle of maximum azimuth error = 2.2 deg
Error wedge = 6.4 deg

(See Fig. 3-1.)

3.1 Magnitude and Extent of Azimuth Error

The maximum azimuth error is determined by the range and width of the obstacle casting the shadow (see Fig. 3-2), e.g., a 100λ wide obstacle at a 20,000 λ range produces a maximum azimuth error of 0.25 degree. In fact, obstacles that produce the same maximum azimuth error have a width given by

$$\text{Obstacle width} = L \times (\text{obstacle range})^{P} \qquad (3.1)$$

for obstacle range > 1000 λ

and obstacle width > 20 λ

where L and P are parameters

The parameters, L and P, are defined in Table 3-1 for three values of maximum azimuth error of 0.25, 0.5, and 1.0 degree.

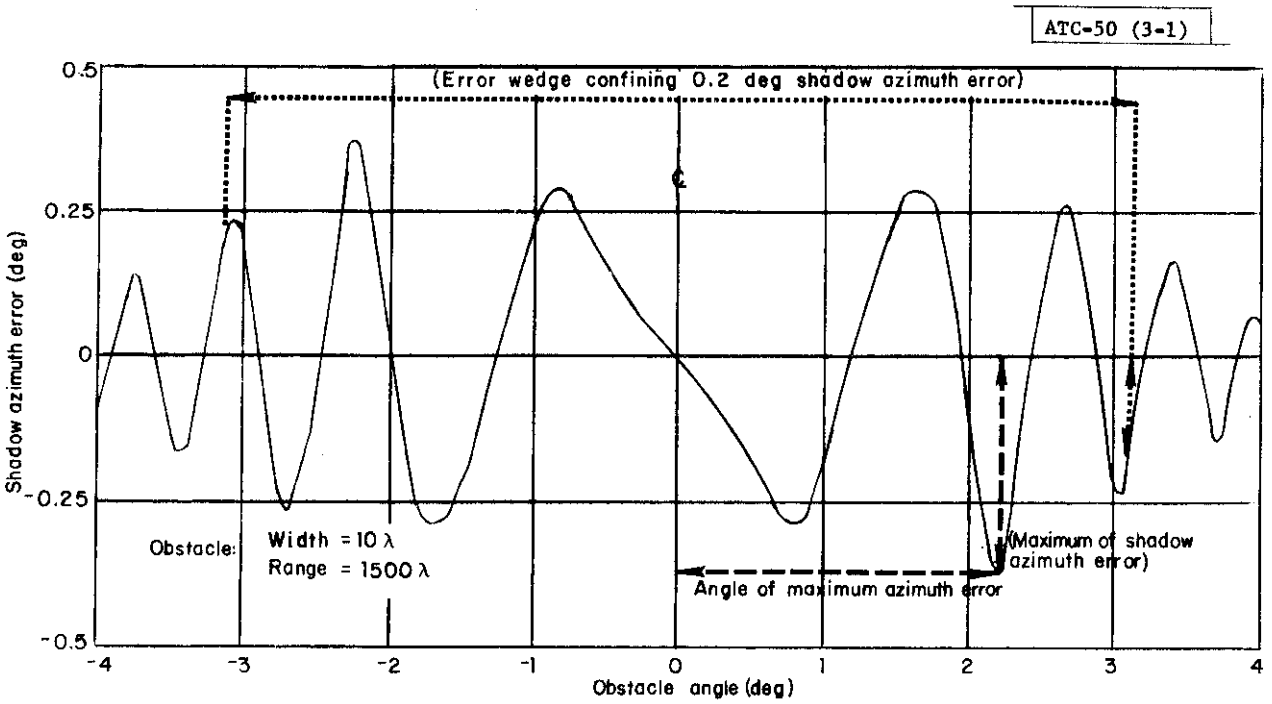

Fig. 3-1. Shadow azimuth error vs obstacle angle (illustration of key features of spatial distribution of the error).

TABLE 3-1.

PARAMETERS OF EQUATION 3.1

Maximum Azimuth Error (deg)	L	P
0.25	0.022	0.85
0.5	0.06	0.79
1.0	0.34	0.69

A constant shadow signal strength is produced by obstacles with a range given in equation 3.1 with P = 0.5. The farther away from the sensor are the obstacles with the same shadow strength, their shadow beamwidth is more narrow. The obstacle width, which determines the beamwidth of the shadow, is the predominant factor in determining the angle of maximum azimuth error (see Fig. 3-3). For example, a 100 λ wide obstacle at a 16,000 λ range has an angle of maximum azimuth error of 0.2 degree, and at a range of 4,000 λ an angle of maximum azimuth error of 0.3 degree. As would be expected, the value of the angle of maximum azimuth error is inversely related to the obstacle width. Specifically a good approximation to the angle of maximum azimuth error is

$$\text{angle of maximum azimuth error} = \frac{20}{\text{obstacle width}} \text{ (deg)} \qquad (3.2)$$

At optical frequencies, the azimuth extent of an opaque obstacle shadow is practically equal to the geometrical azimuth extent of the obstacle. At DABS downlink frequency, 1090 MHz, there is no simple relationship between the obstacle geometrical azimuth extent and the error wedge, which is the azimuth extent where the RF shadow corrupts the azimuth estimation.

Error wedge, as a function of obstacle width for five different obstacle ranges, is given in Figs. 3-4 and 3-5. Also plotted is the azimuth extent (geometrical) of the obstacle at the sensor. For a given obstacle range, there is a minimum obstacle width (for example at a range of 4000 λ, the minimum width is 10 λ) below which, error wedge is zero, a consequence of equation 3.1. Obstacles wider than this minimum width cast a shadow strong enough to cause an azimuth error of 0.2 degree, thereby setting the error wedge to a nonzero value; but a further increase in obstacle width reduces the shadow beam width and reduces the error wedge with it. A continued increase in obstacle width introduces strong sidelobes of the shadow, suddenly increasing the error wedge. (In Fig. 3-4, at an obstacle range of 4000 λ, the first sidelobe becomes strong enough to cause a shadow azimuth error of 0.2 degree; when the obstacle width = 44 λ, the error wedge increases from 2 to 4 degrees.)

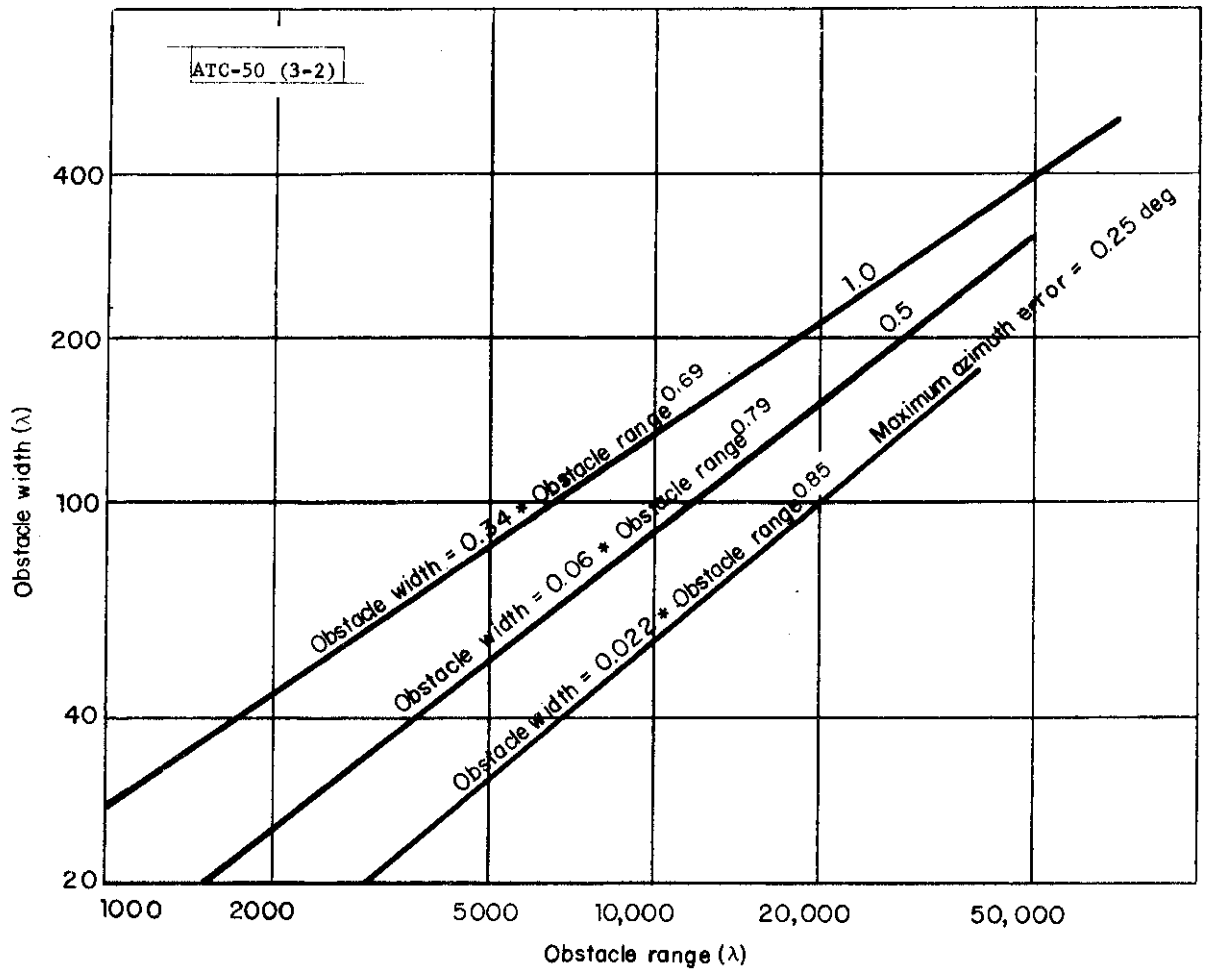

Fig. 3-2. Maximum azimuth error (deg) as a function of obstacle width (λ) and range (λ).

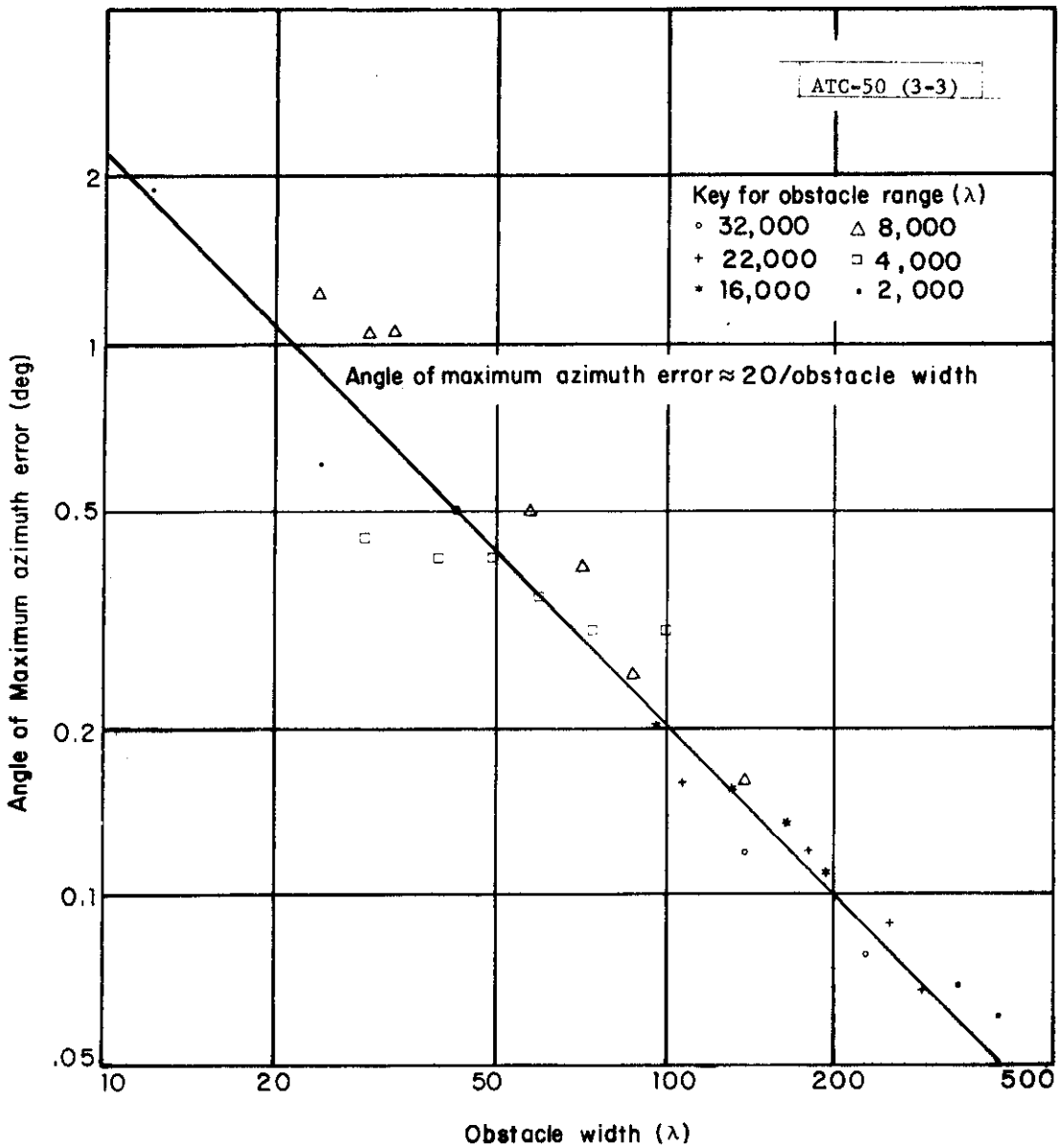

Fig. 3-3. Angle at off the center of obstacle where peak azimuth error occurs vs obstacle width (\) and range (\).

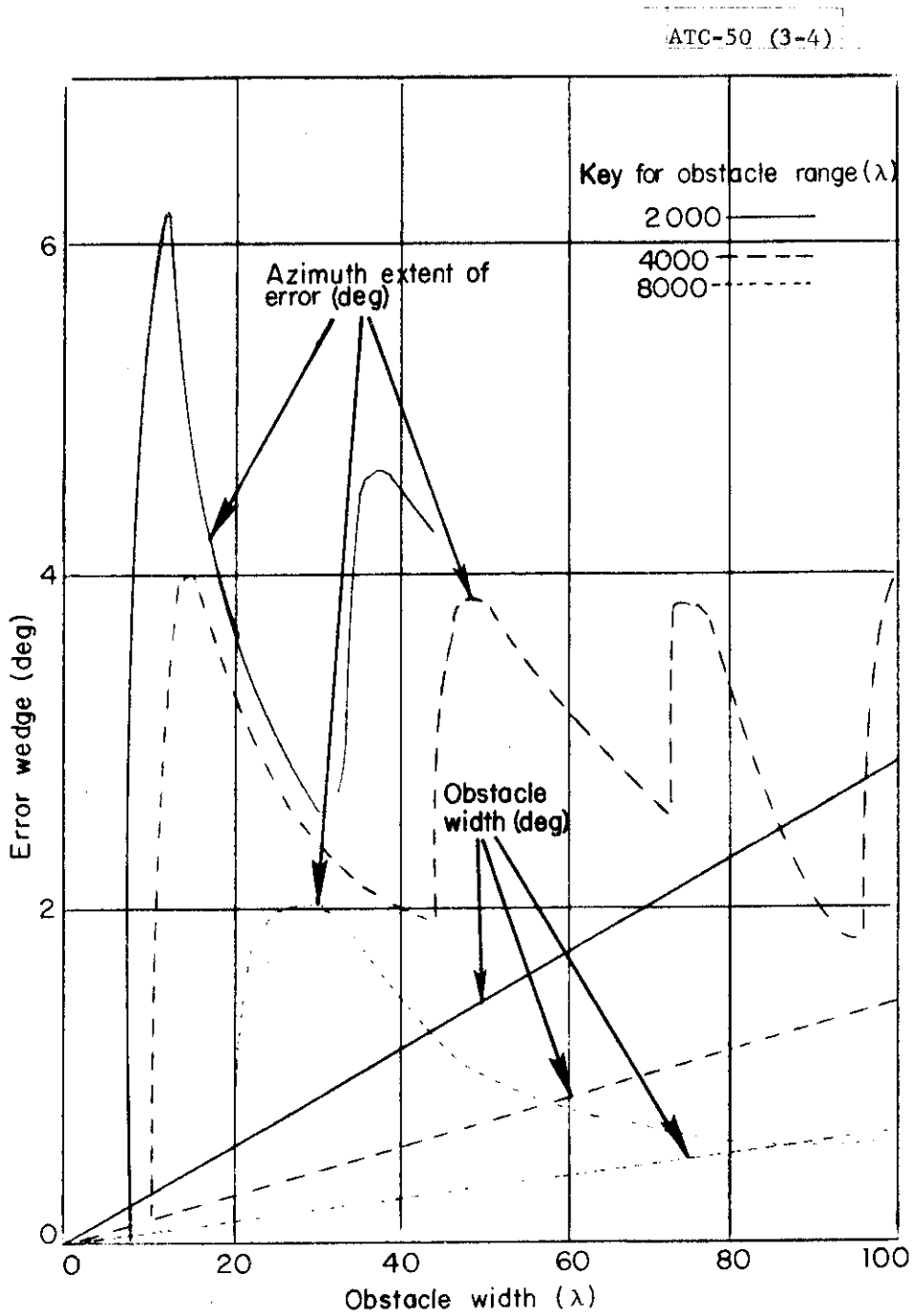

Fig. 3-4. Error azimuth extent vs obstacle parameters: range and width.

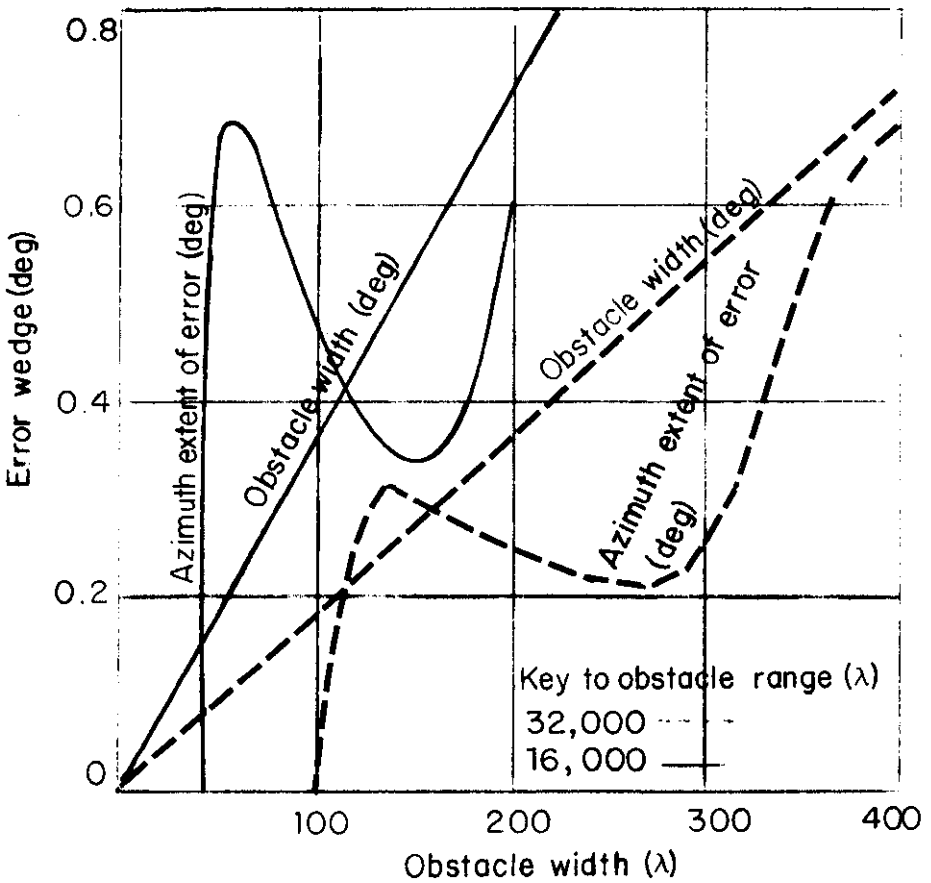

Fig. 3-5. Error azimuth extent vs obstacle parameters: range and width.

3.2 Change of Azimuth Error With Modification of Operating Conditions

Nominal operating conditions are not met all the time. The effect of modification of three operating conditions is of interest: (1) range of the aircraft, (2) elevation of the aircraft, and (3) shape of the obstacle.

3.2.1 Aircraft Range

A big shadow azimuth error is produced when the aircraft is close to the obstacle shadowing it. The azimuth error is evaluated for an aircraft at three ranges (Fig. 3-6). Maximum azimuth error increased from 0.25 deg to 0.55 deg when the aircraft range is 64,000 λ as compared to very long range. The azimuth error for an aircraft flying out on a radial stays practically the same, once the aircraft goes beyond a range 10 times the obstacle range. (See Appendix B for further details regarding this section.)

3.2.2 Aircraft Elevation

Not all obstacles are necessarily very tall to completely block the field from diffracting over their tops to the aircraft. An aircraft elevation close to the top of the obstacle will have a smaller azimuth error than it has at low elevations. For purposes of illustrating this effect, the Envelope of Azimuth Error is defined as the locus of the peaks of Shadow Azimuth Error as a function of obstacle angle (see Fig. 3-7). A plot of Envelope of Azimuth Errors for three aircraft elevations (well below the top of an obstacle, slightly skimming the top of an obstacle, and above the top of an obstacle) is shown in Fig. 3-7. In general, as well as can be specifically noted in the present example, the maximum azimuth error with the aircraft slightly above the top of the obstacle is about a half of maximum azimuth error with the aircraft at very low elevation. Furthermore, an aircraft elevation above the top of the obstacle by E_c deg where

$$E_c > \tan^{-1} \sqrt{\frac{2\lambda}{\text{obstacle range}}} \qquad (3.3)$$

experiences a small shadow azimuth error. For an obstacle at 6,000 λ range, E_c is one degree.

3.2.3 Obstacle Shape

The skyline could be formed by complex shaped obstacles; it is not always made up of isolated rectangular obstacles such as smokestacks or buildings. The spatial distribution of shadow azimuth error produced by 'complex' shaped obstacles departs markedly from the 'simple' distribution corresponding to isolated obstacles. Such an example is the shadow azimuth error produced at DABSEF antenna by the shadow of an obstacle within 500 λ range (see Figs. 3-8 and 3-9). The variety of shadow azimuth error distribution is then as great as the variety of sensor skylines.

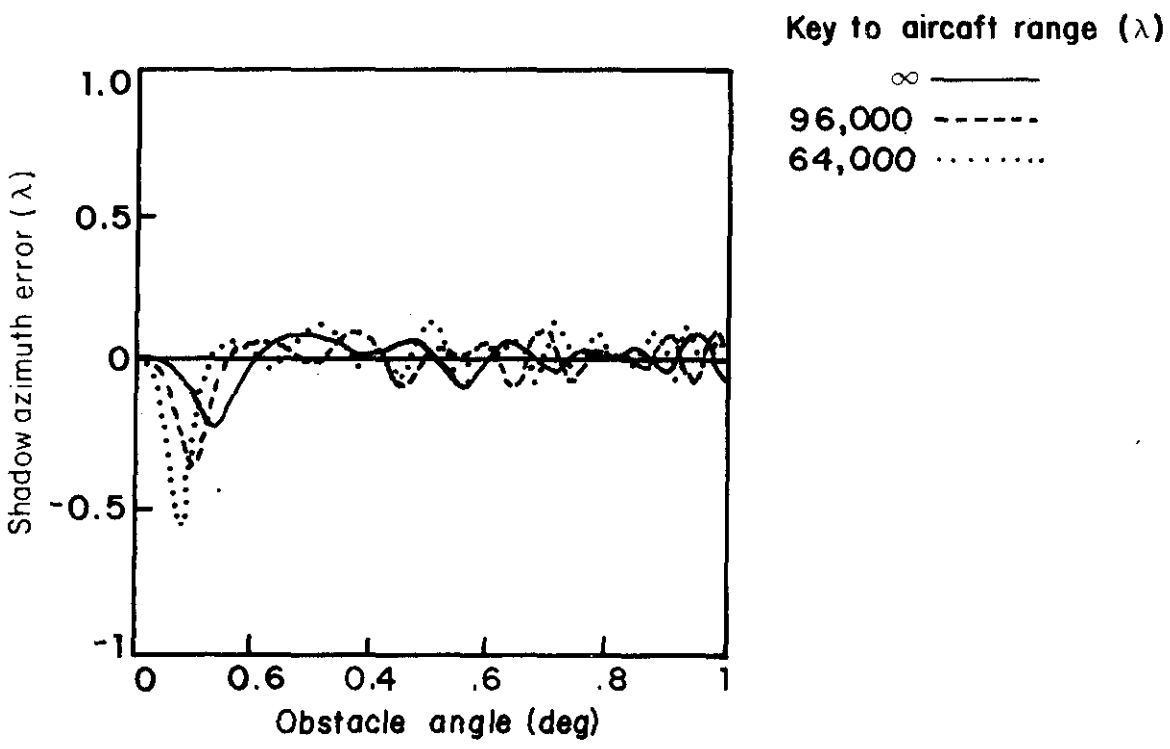

Fig. 3-6. Shadow azimuth error vs obstacle azimuth for an aircraft at 3 ranges; obstacle is at 32, 000 λ range, is 140 λ wide.

ATC-50 (3-7)

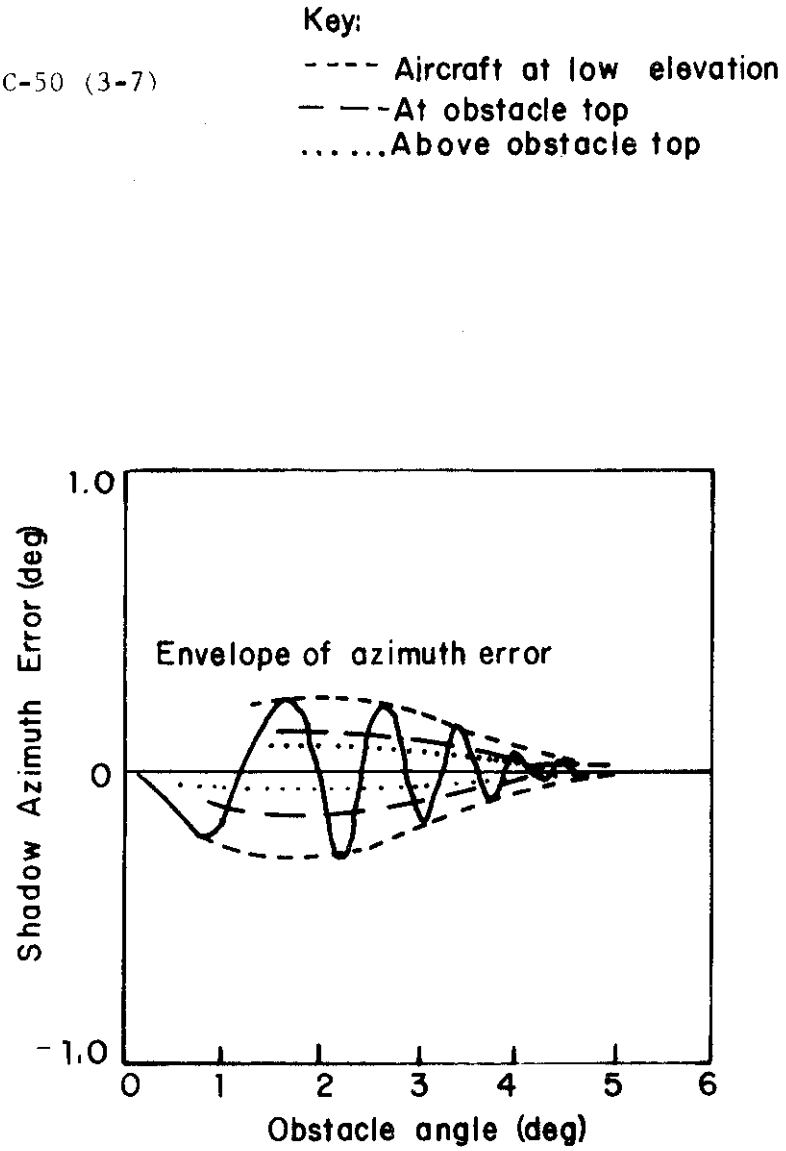

Fig. 3-7. Envelope of azimuth error vs obstacle azimuth.

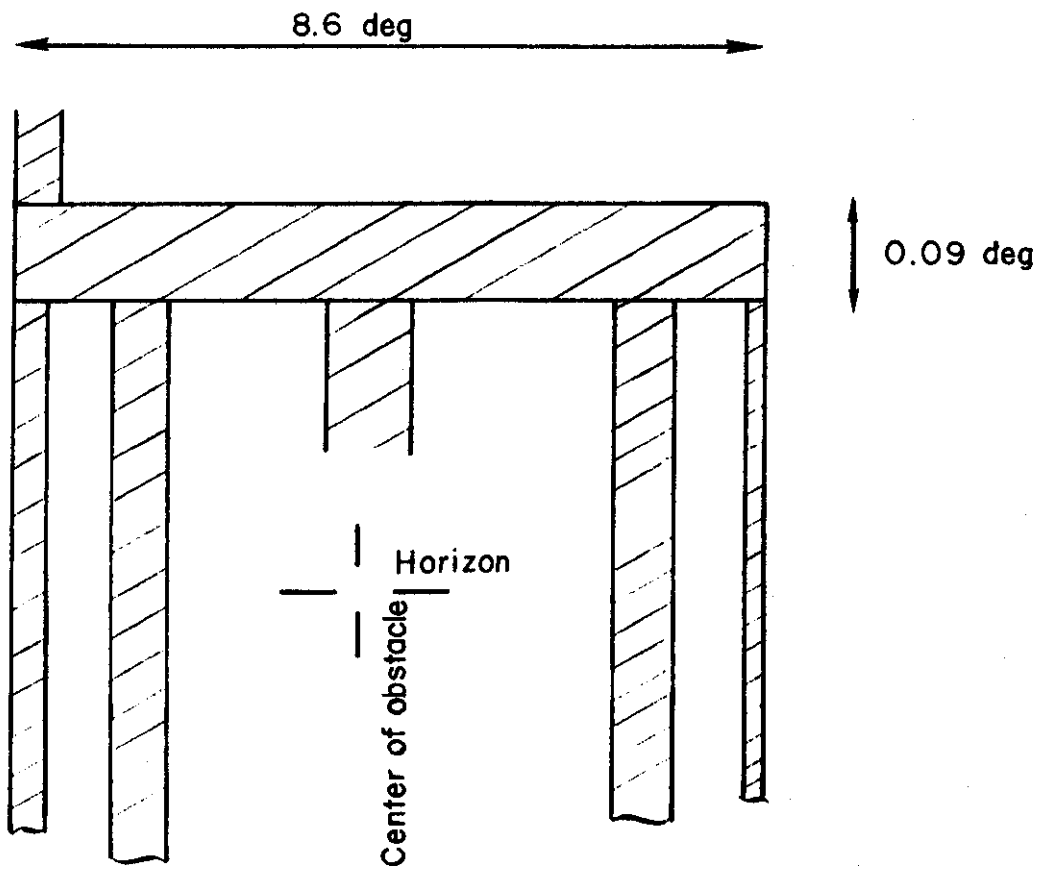

Fig. 3-8. Shape of complex obstacle as seen from sensor; obstacle range is 500 .

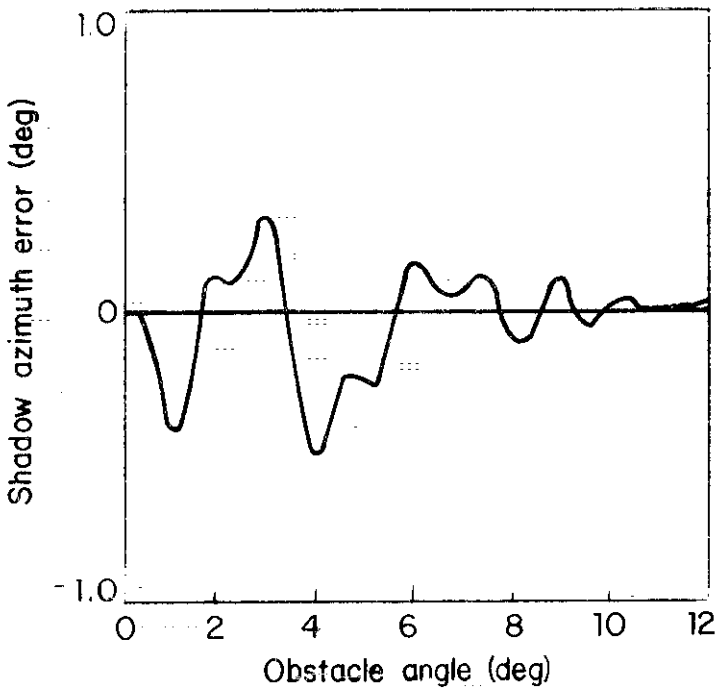

Fig. 3-9. Shadow azimuth error vs obstacle azimuth for the complex obstacle of Fig. 3-9. Aircraft is 2 degrees.

3.3 Summary of Shadow Extent and Magnitude

Most of the characteristics of the shadow induced azimuth error seem plausible. The surprising feature is the introduction of 'error skirts' spanning azimuth wedges much larger than the obstacle extent for close-range obstacles. Important characteristics of the azimuth error in relation to the obstacles producing them are:

(a) In many cases of practical application, a very narrow obstacle will produce very little azimuth error. {For obstacle ranges (R) between 3000 λ and 90,000 λ, and aircraft ranges much greater than obstacle range; an azimuth error of less than 1/4 degree will be produced by an obstacle whose width is less than $.02\ R^{.85}$ (R in wavelengths, λ)}.

(b) The peak azimuth error moves closer to the obstacle center in azimuth, the wider the obstacle is. A good approximation of the angle of maximum azimuth error (deg) is 20/width of obstacle (λ).

(c) Obstacles that are at close range and appear to be narrow in azimuth extent (less 0.5 deg) can produce azimuth errors greater than 0.2 deg over large azimuth wedges, e.g., 4 degrees (see Fig. 3-4).

(d) For obstacle ranges $5000\ \lambda \leq R \leq 30,000\ \lambda$, errors greater than $.2^{o}$ occur within an azimuth wedge approximately equal to the obstacle azimuth extent, when azimuth extent $> 3^{o}$. At longer ranges, $R > 30,000\ \lambda$, the 3^{o} limit does not apply.

(e) A short obstacle (in height) will interfere with the azimuth estimate by a smaller extent than a tall obstacle; for narrow obstacles (e.g., Hanscom smokestack), when the obstacle top just reaches the line joining the sensor to the aircraft, the azimuth error will be about half that corresponding to a very tall (narrow) obstacle.

(f) When the line of sight is physically blocked by an obstacle, aircraft close to the obstacle shadowing them experience a larger azimuth error than those far removed.

(g) Obstacles, with the same azimuth extent at the sensor, will cause a larger azimuth error the farther they are away from the sensor.

4.0 ERROR SENSITIVITY TO ANTENNA APERTURE AND ANGLE ESTIMATION PROCESSING

When obstacles block the view of a sensor site, two legitimate questions are

(1) How does the monopulse angle estimate compare with the sliding window (an angle estimate used in ARTS)?

(2) Does increasing the width of the antenna reduce the severity of the shadow azimuth error?

The answer to the first question is that the azimuth error in the monopulse estimate is comparable to that of the sliding window. As for the second question, the antenna width produces very little change in the azimuth error in most cases.

4.1 Comparison of Sliding Window With Monopulse Azimuth Error

For the purpose of comparison, the sliding window angle estimate is modeled as the azimuth corresponding to the center of a window spanning the sum beam at a fixed power, threshold (dB), below its peak; details of the procedure are given in Appendix A. Consider shadow azimuth error as a function of obstacle angle (shown in Figs. 4-1 and 4-2) for the Hanscom smokestack and the Prudential building (the examples used in Chapter 1). It is seen that the maximum azimuth error of the sliding window is within 25% of that of the monopulse. In the above examples, a 12-dB threshold is used. An increase in threshold, by reducing the threshold for accepting replies, would increase the shadow azimuth error (see Figs. 4-3 and 4-4).

In actual operation the sliding window angle estimate includes an error component caused by missed replies of the edges of the window and quantization error produced by the finite PRF. For the purpose of illustration, consider a PRF of 250 interrogations/sec and a rotator rpm of 15, the quantization error is 0.2 deg, a value that helps to put the sliding window estimate at a disadvantage with respect to monopulse, especially if the shadow azimuth error is a fraction of a degree. Of course, a PRF of 400 would decrease the quantization error to approximately 0.1 deg.

4.2 Effect of Antenna Horizontal Aperture on Azimuth Error

For most obstacles, the antenna horizontal aperture (ceiling within a factor of $\pm$ 2) has little effect on azimuth error. Exceptions to this statement are that for an obstacle at a range less than a few thousand λ, a wide aperture reduces the azimuth error; for obstacles at a range less than 10,000 λ, an increase of aperture reduces the volume of space where there would be error. At first, the small effect of antenna aperture on azimuth error of obstacles at long range seems to be counterintuitive; however, note the following:

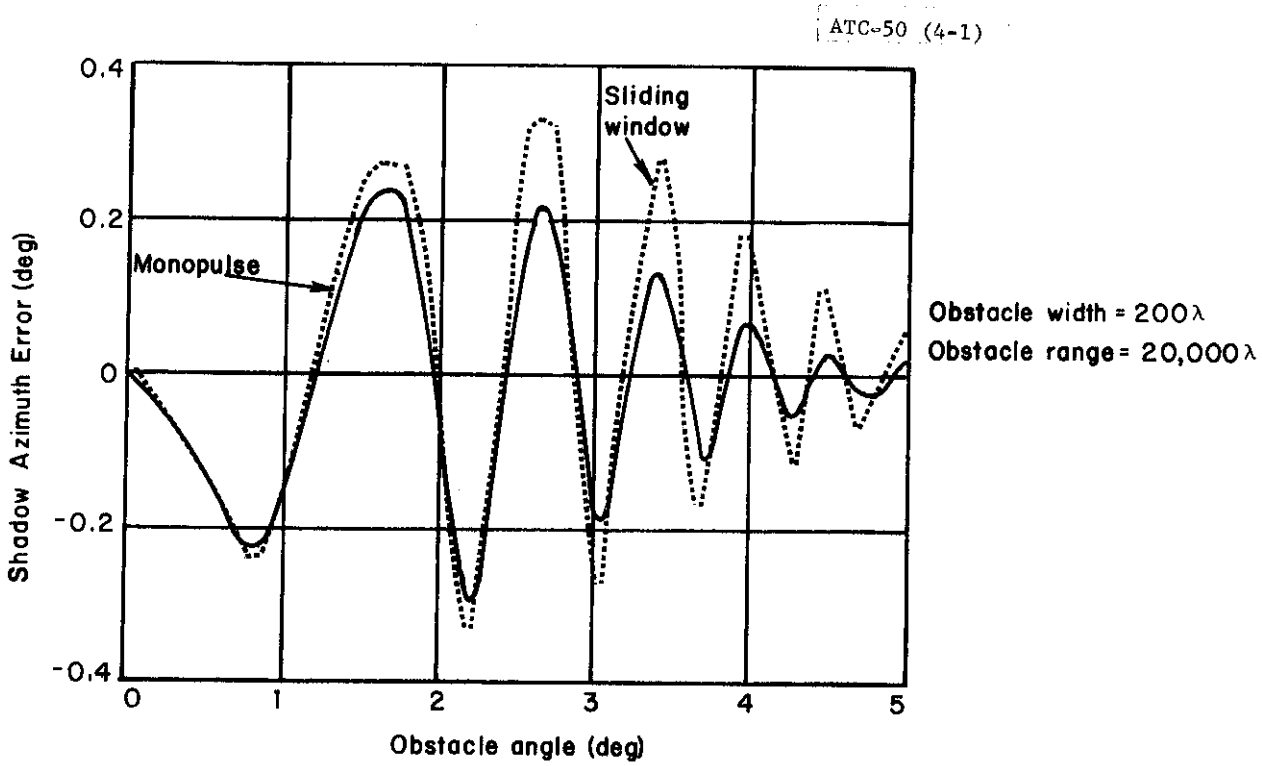

Fig. 4-1. Hanscom smokestack azimuth error; comparison between sliding window (threshold 12 dB below peak) and monopulse.

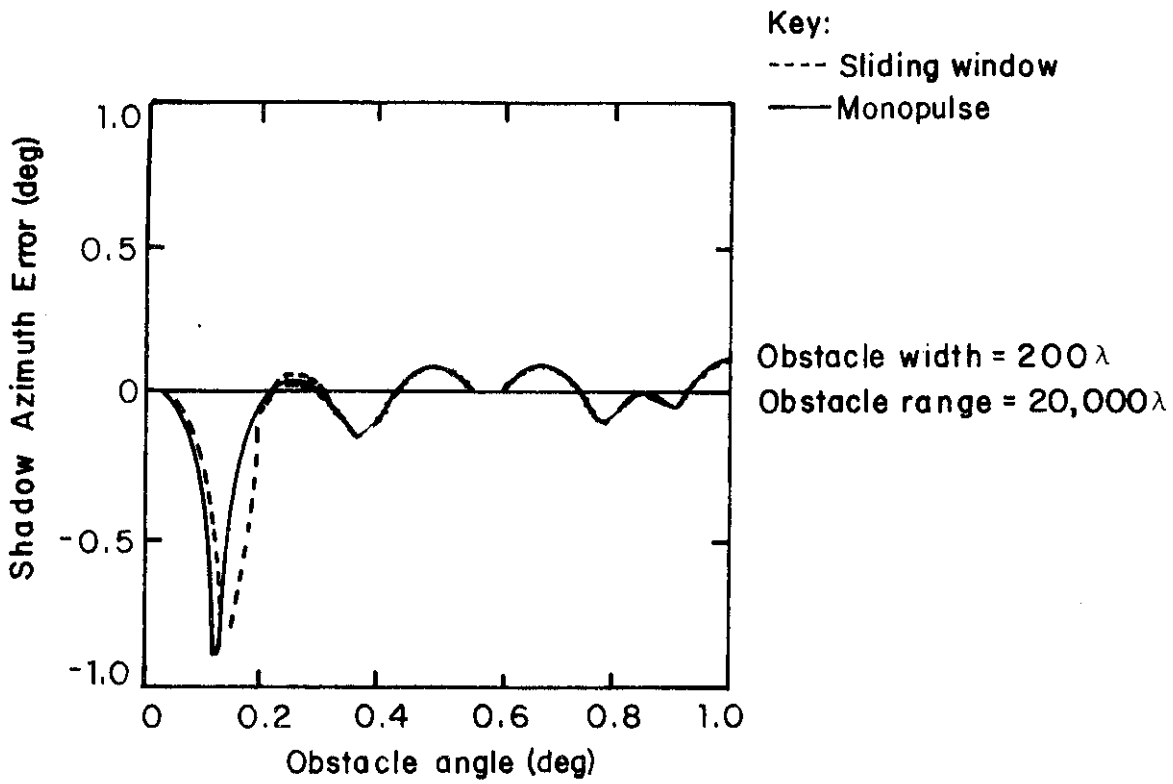

Fig. 4-2. Prudential building shadow azimuth error; comparison between sliding window (threshold 12 dB below peak) and monopulse.

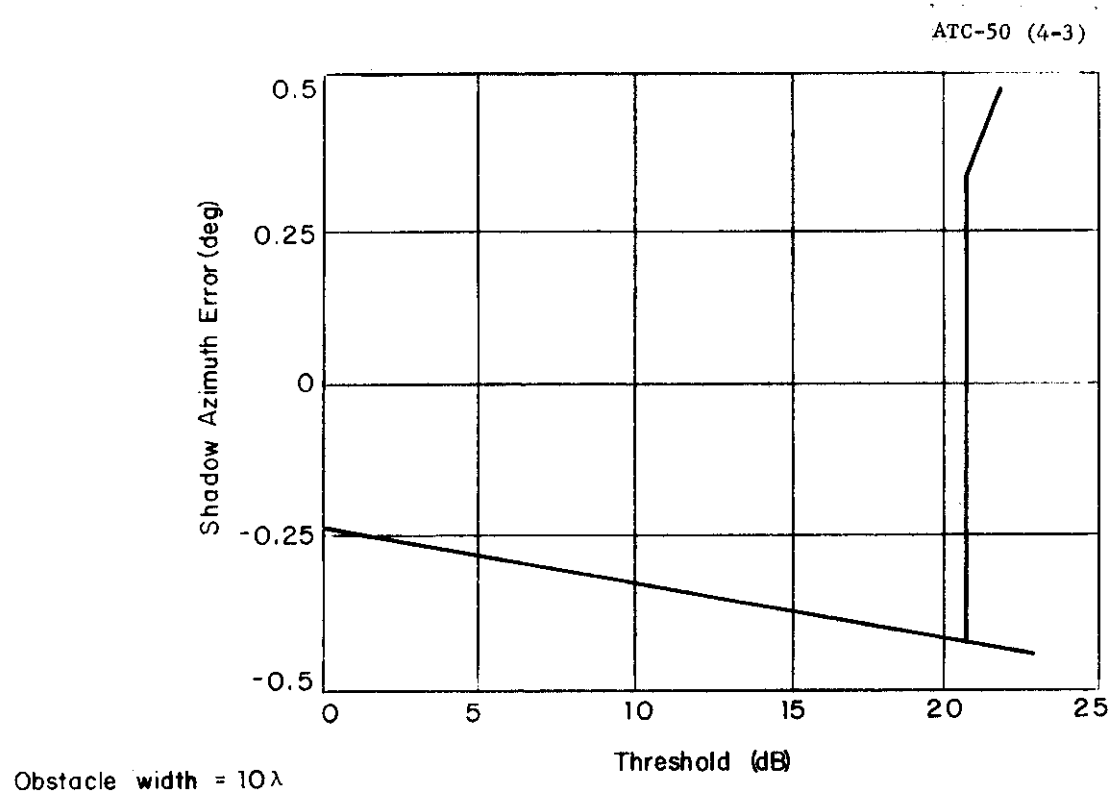

Fig. 4-3. Sliding window azimuth error vs threshold; obstacle is the Hanscom smokestack.

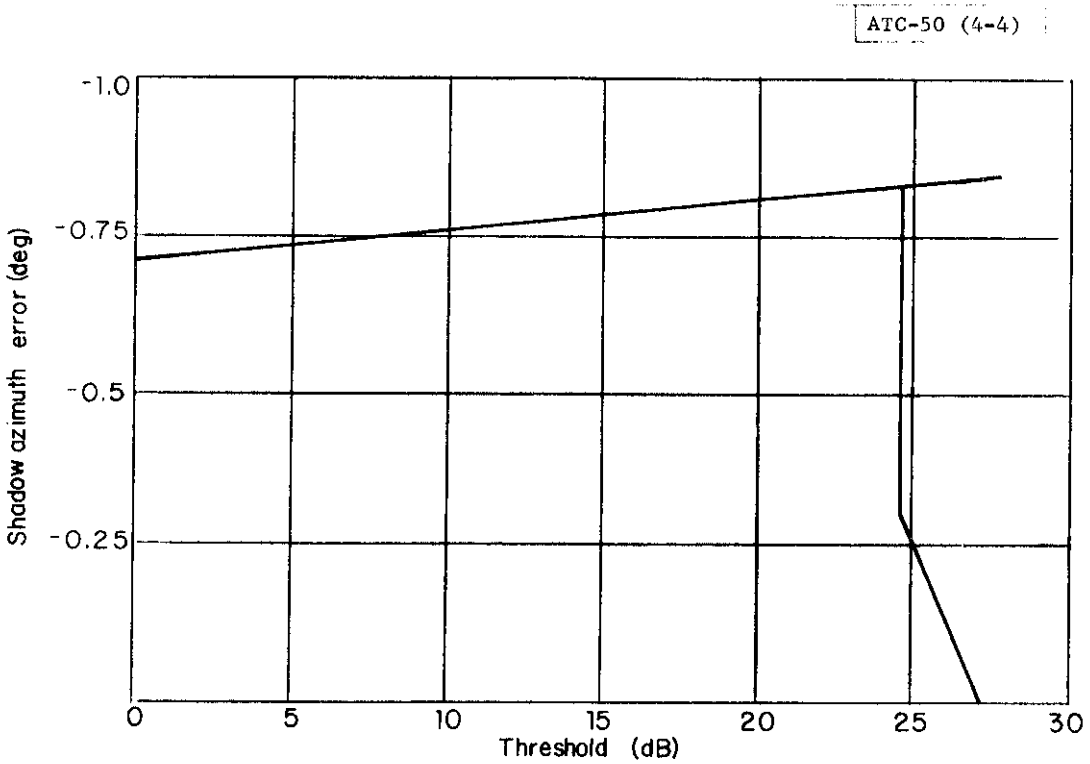

Fig. 4-4. Sliding window azimuth error vs threshold; obstacle is Prudential building.

(1) Obstacles at long range that cause significant azimuth error are wide, and their shadow beamwidth is much more narrow than 1.5 degrees, which is one-half the nominal antenna beamwidth.

(2) An obstacle maximum azimuth error occurs at a 'fixed' angle off the antenna boresight.

(3) An interferor at a fixed off-boresight angle within the antenna beamwidth causes the same error independent of the aperture width [Ref. 1.]

The relative insensitivity to aperture width of the azimuth error extent is explained by note 1, while that of the azimuth error magnitude is explained by notes 2 and 3.

The DABSEF antenna illumination (which is 22 λ wide) was scaled to apertures 44 λ wide and 11 λ wide. These double and half normal apertures were used to estimate the azimuth. The resulting azimuth errors for some typical situations, which illustrate the effect of antenna width on azimuth error, are given in Table 4.1 and Figs. 4-5 and 4-6.

TABLE 4-1. APERTURE EFFECT ON AZIMUTH ERROR

Obstacle Width	Range	Error Wedge (deg)			Maximum Azimuth Error (deg)		
		1/2 x Nominal Aperture	Nominal Aperture	2 x Nominal Aperture	1/2 x Nominal Aperture	Nominal Aperture	2 x Nominal Aperture
25	2,000	8.0	3.2	1.6	0.51	0.47	0.39
80	8,000	2.2	1.2	0.8	0.57	0.5	0.47
135	16,000	0.4	0.4	0.4	0.6	0.5	0.49
230	32,000	0.24	0.24	0.24	0.6	0.5	0.51

4.3 Antenna Illumination Pattern Effect on Azimuth Error

The antenna illumination pattern performs a minor function in the shadow azimuth error. A comparison, for the shadow azimuth error, between the modified feed ASR-7* and the DABSEF antenna shows that the difference in the error is less than 0.07 degree (see Figs. 4-7 and 4-8). The method of computing the shadow azimuth for a reflecting dish, using the illumination pattern for the modified ASR-7 as an example, is given in Appendix C.

4.4 Summary of Results

(a) For obstacles 2 or more nmi away, varying the antenna width in values close to 22 λ (e.g., to 11 λ or 30 λ) is

*A reflecting dish antenna with a 17.5 λ aperture width at DABS frequency.

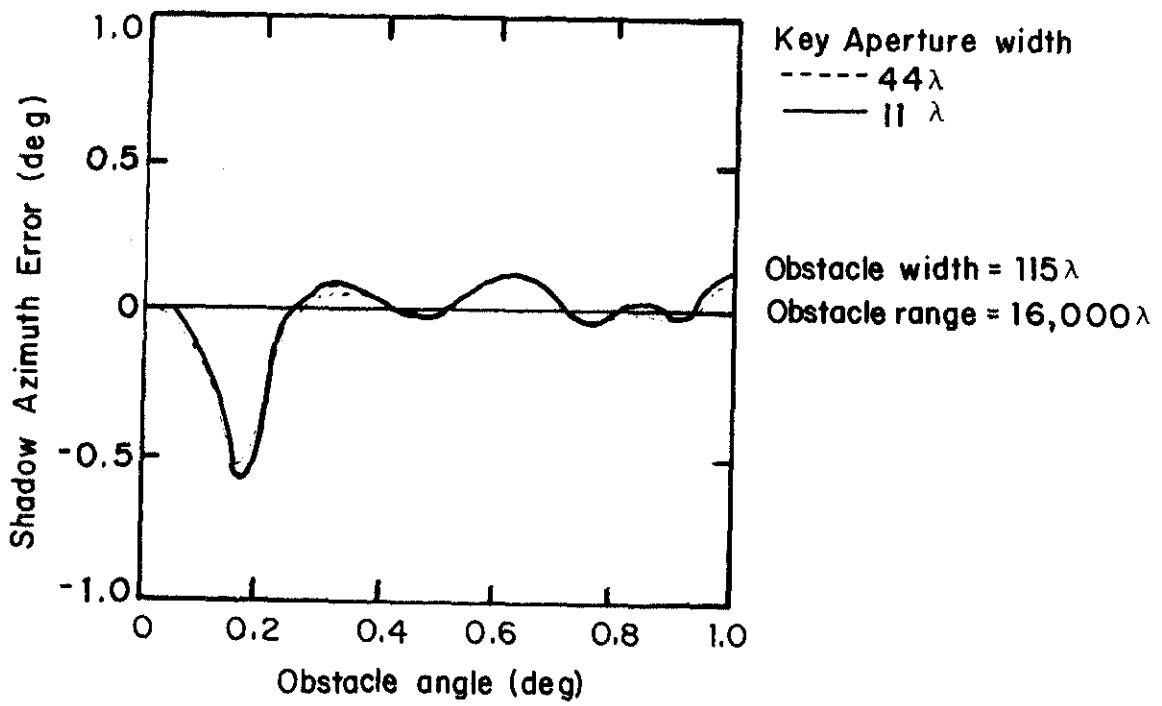

Fig. 4-5. Effect of antenna width on shadow azimuth error vs obstacle angle; obstacle is at long range.

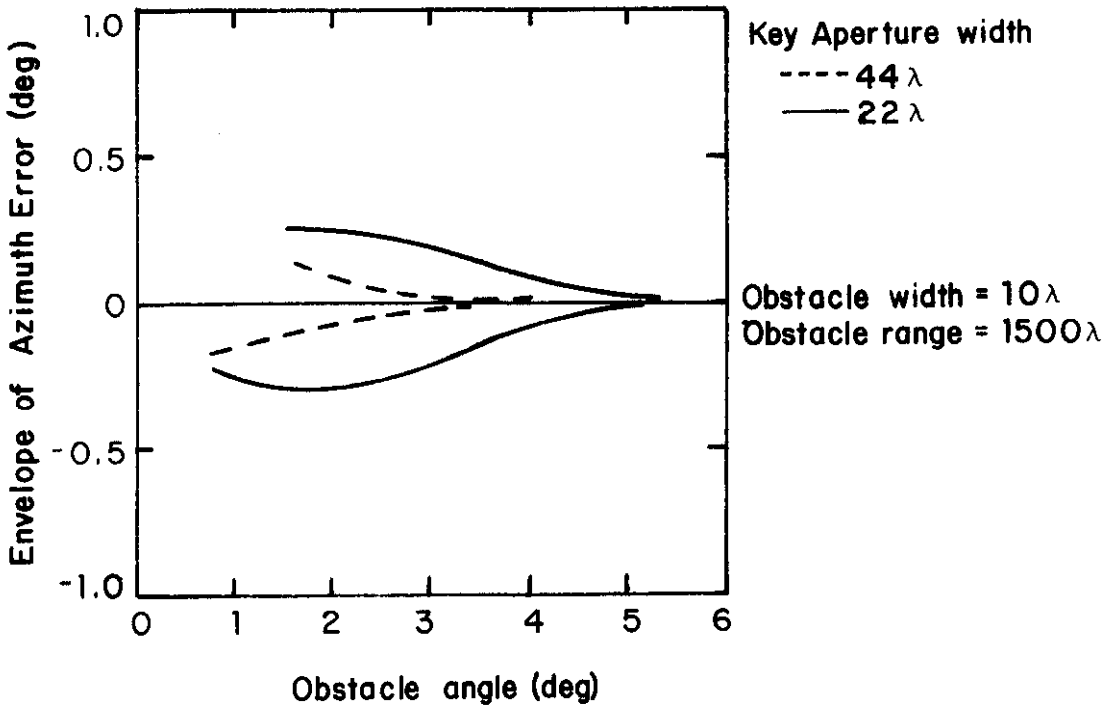

Fig. 4-6. Effect of antenna width on envelope of azimuth error vs obstacle angle; obstacle is at close range.

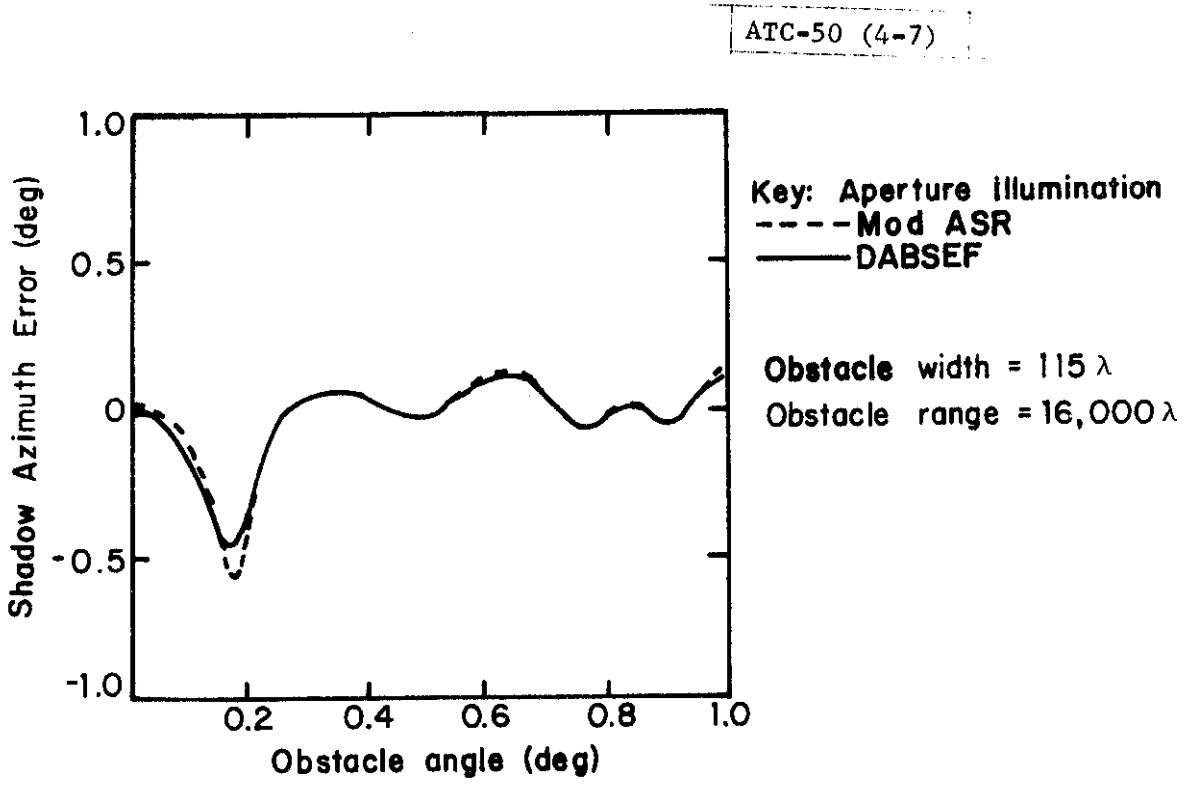

Fig. 4-7. Effect of antenna illumination on shadow azimuth error vs obstacle angle; obstacle is at long range

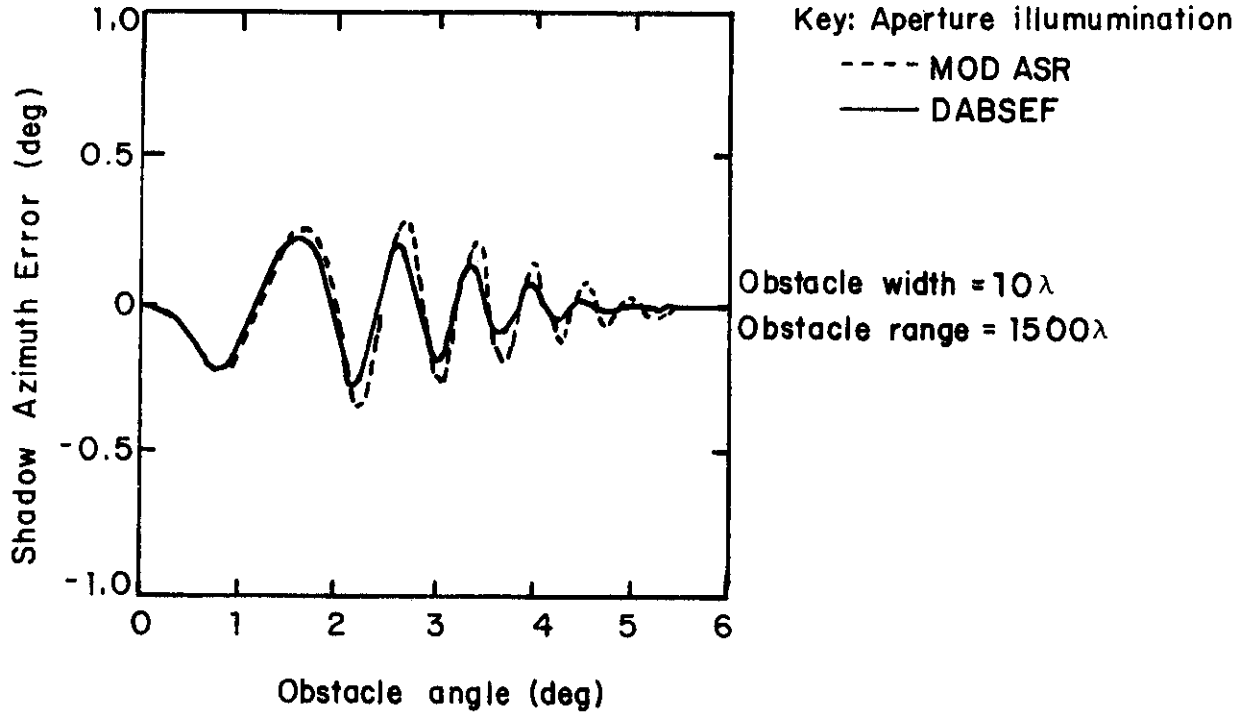

Fig. 4-8. Effect of antenna illumination on shadow azimuth error vs obstacle angle; obstacle is at close range.

not going to affect the shadow azimuth error with on boresight monopulse or beam splitting.

(b) For on boresight monopulse or beam splitting and obstacles at very close range (less than 2000 λ), an increase of the antenna width from 22 λ to 44 λ reduces the extent and magnitude of the shadow azimuth error for narrow obstacles.

(c) The on boresight monopulse estimate azimuth error is comparable to a beam splitting azimuth error. If the quantization error of beam splitting, caused by finite PRF is taken into consideration, monopulse azimuth error is smaller.

(d) Shadow azimuth error is a weak function of antenna illumination pattern.

5.0 AZIMUTH ERROR CHARACTERISTICS RELATED TO SENSOR DATA PROCESSING

Presented in this section are two characteristics of the azimuth error that interact strongly with the sensor data processing in determining the surveillance quality provided by DABS: (1) the spatial variation of azimuth error magnitude, and (2) the sensitivity of azimuth error to aircraft off-boresight angle.

5.1 'Oscillation' of Azimuth Error

An obstacle at long range from the sensor will produce a more rapid variation of azimuth error with azimuth compared to obstacles at close range. The sensitivity of azimuth error oscillation to obstacle range is well illustrated by considering the azimuth error produced by an obstacle at two ranges (Fig. 5-1). The obstacle angles, where the shadow azimuth error crosses a value of zero, are

$$\pm \tan^{-1} \sqrt{\frac{n}{R}} \qquad (5.1)$$

where n = 0, 1, 2, 3...

An aircraft moving across range will experience a greater variation in azimuth error on successive scans compared to an aircraft moving along a radial from the sensor.

5.2 Azimuth Error at Off-Boresight Interrogations

The azimuth error magnitude changes with the aircraft off-boresight angle. With the obstacle at a negative angle relative to the aircraft, interrogations to the aircraft at a leading edge of a beam sweeping clockwise produce a larger azimuth error than interrogations at the trailing edge. For example, with the Hanscom smokestack at -2.2 degrees from the aircraft, the shadow azimuth error is 0.67 degree with the aircraft at 2.4 degrees off-boresight as compared with the shadow azimuth error of 0.1 degree with the aircraft at -2.4 degrees off-boresight (see Figs. 5-2 through 5-4). If, by symmetry, the shadowing obstacle is at a positive angle relative to the aircraft, leading edge interrogations experience a smaller error than interrogations at the trailing edge of the beam. The change in azimuth error with off-boresight angle is more pronounced the larger the azimuth separation of the aircraft from the obstacles shadowing them.

Consider a fixed beamwidth of the antenna, e.g., 4.8 degrees and approximately a 2-degree fixed separation between the obstacle and aircraft, then two features of the azimuth error vs the off-boresight angle are

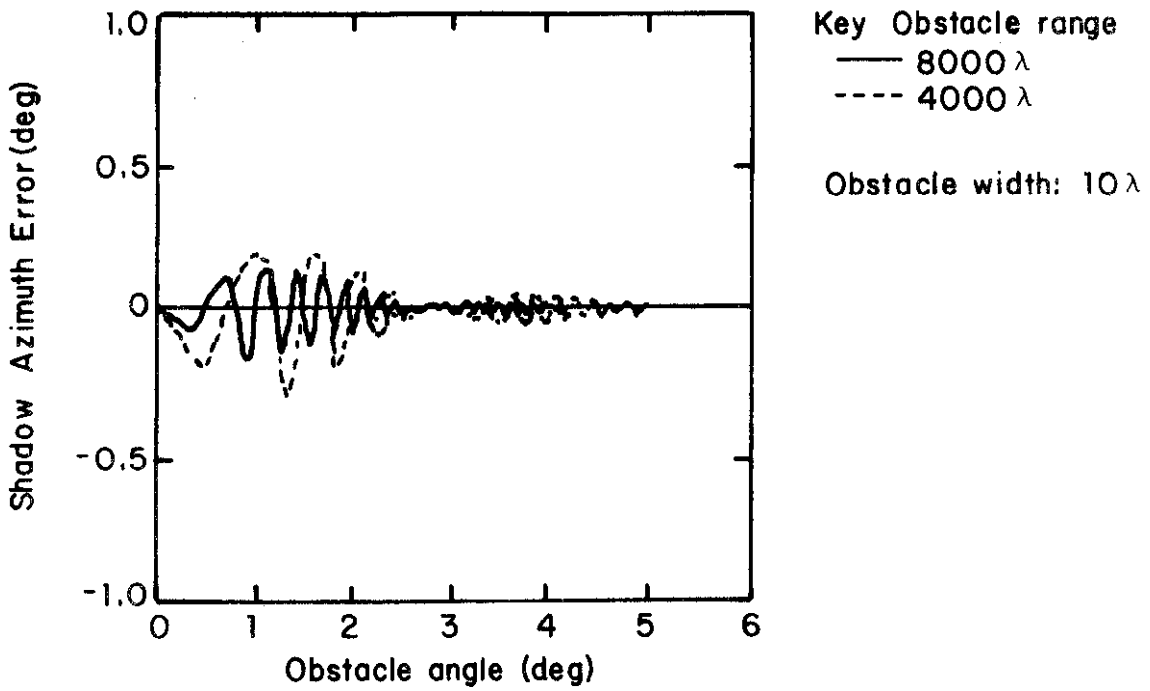

Fig. 5-1. Spatial oscillation of azimuth error vs obstacle angle for two obstacle ranges.

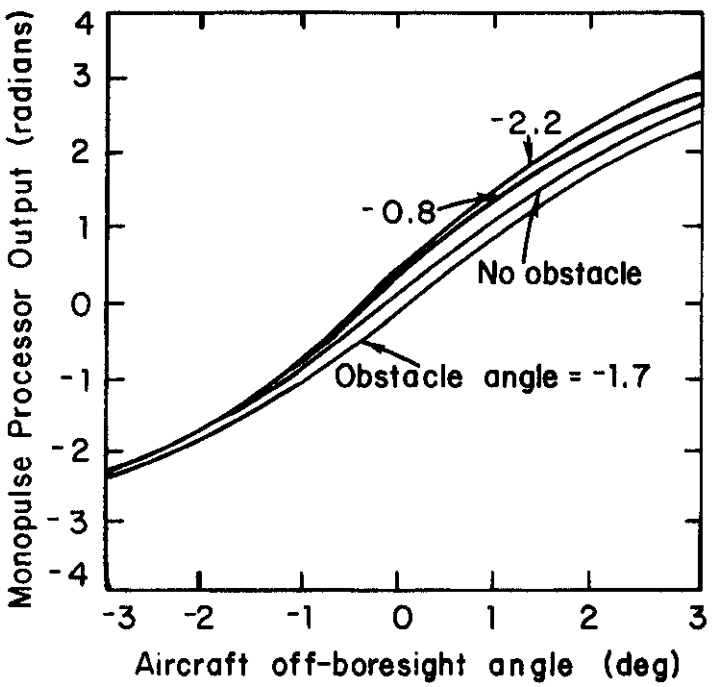

Fig. 5-2. Monopulse output vs off-boresight angle of aircraft; sensitivity to obstacle position.

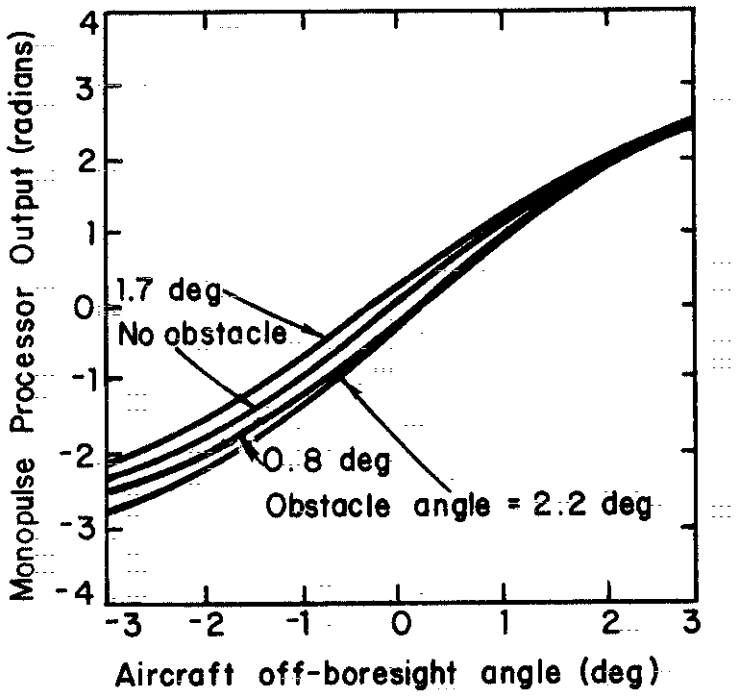

Fig. 5-3. Monopulse output vs off-boresight angle of aircraft; sensitivity to obstacle position.

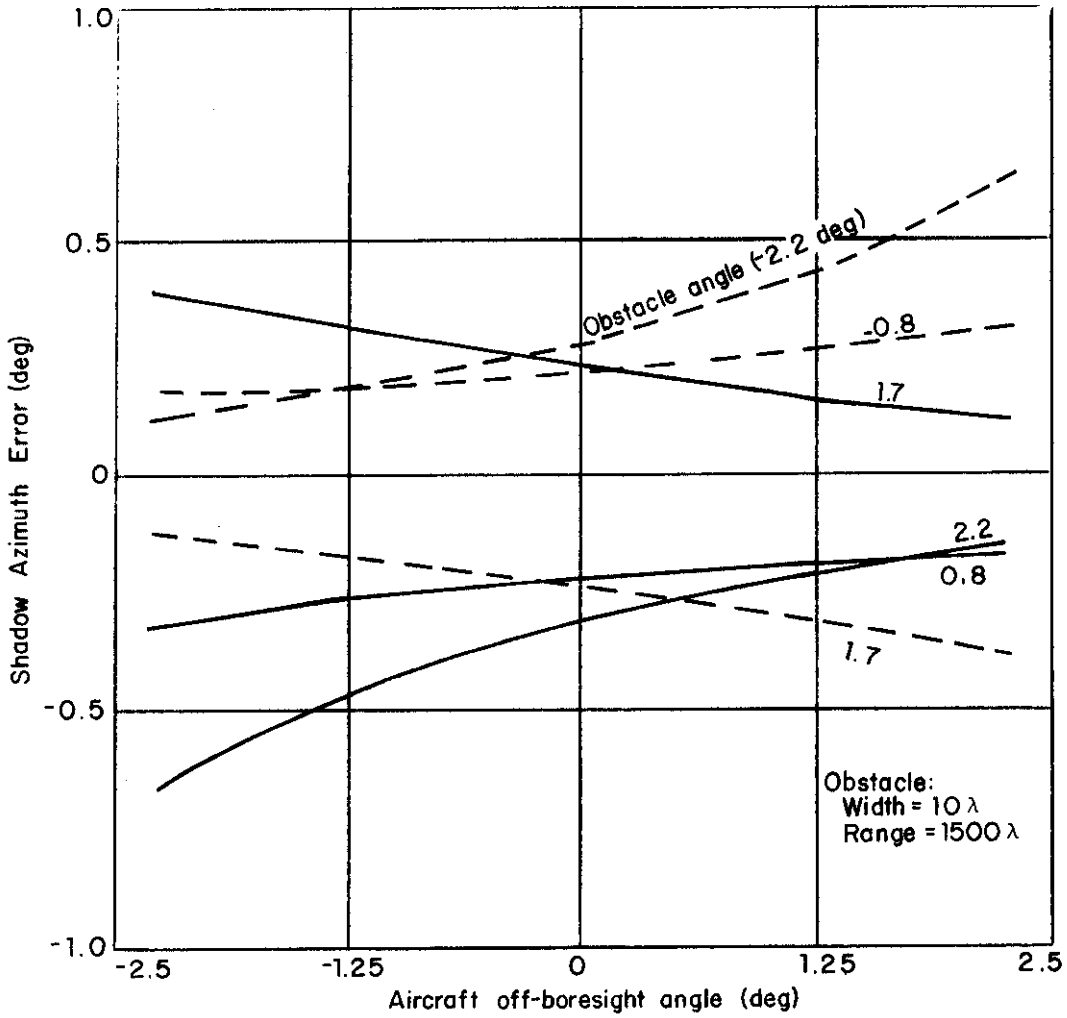

Fig. 5-4. Azimuth error vs off-boresight angle of aircraft for different obstacle positions.

(1) The shadow azimuth error varies at a constant rate with the off-boresight angle.

(2) The ratio of the minimum magnitude of the shadow azimuth error to its maximum magnitude is relatively independent of obstacle position and dimension (see Fig. 5-5).

If the separation between the obstacle and the aircraft is reduced, then in item (2) above, the ratio will go up, e.g., a decrease of the separation of the Hanscom smokestack from the aircraft from 2.2 degrees to 0.8 degree increases the ratio of minimum error to maximum error from 0.15 to 0.4 for a 4.8-degree beam width.

5.3 Summary and Conclusions

To reduce azimuth error, interrogation at the leading (trailing) edge of the beam is preferable if the beam sweeps by the aircraft before (after) the obstacle. Frequency of oscillation of the azimuth error vs azimuth is

(1) Proportional to (obstacle range)$^{1/2}$

(2) Higher at azimuth further removed from the obstacle center.

Azimuth error varies with aircraft off-boresight angle. If the error is normalized with respect to its greatest value over a fixed 'beam width', then the rate of variation with off-boresight angle is

(1) Constant for obstacles of different width and range that fall at a fixed azimuth separation from the aircraft

(2) Faster for obstacles more removed in azimuth from the aircraft.

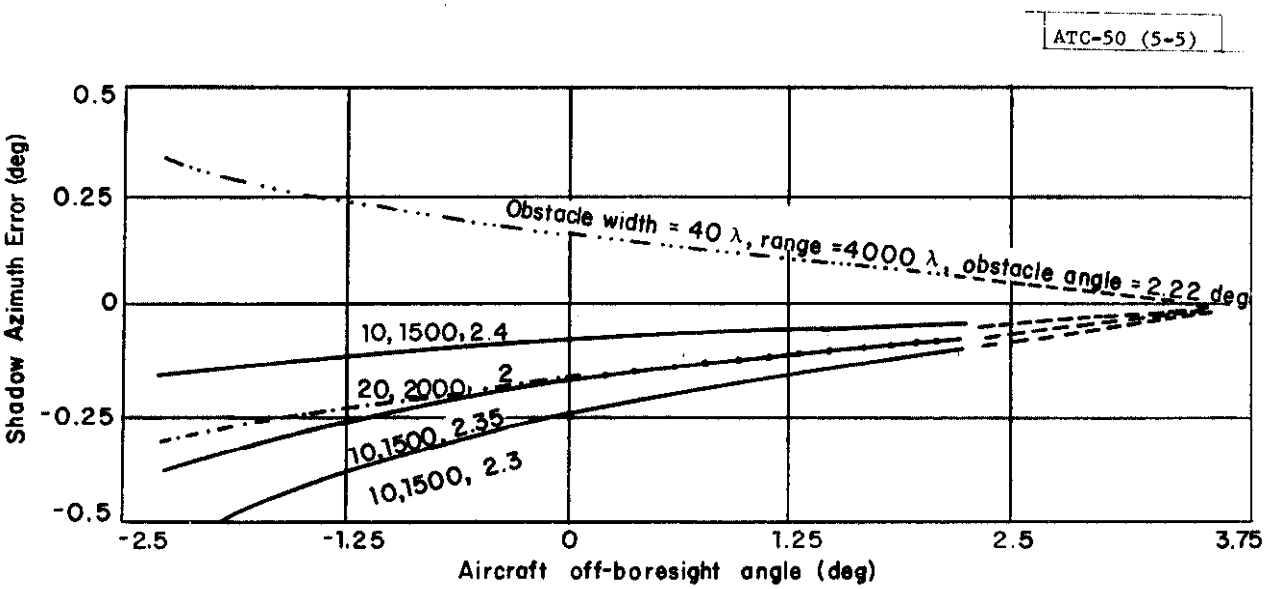

Fig. 5-5. Drop of azimuth error vs aircraft off-boresight angle; obstacles are 2 degrees away in azimuth from aircraft.

APPENDIX A

A. 1 Method of Computing the Monopulse Azimuth Error

The monopulse processor output determines the azimuth error; the azimuth error of a target is equal to the difference between the target off-boresight angle, T, and the angle in the monopulse calibration curve corresponding to the monopulse processor output (MO). The calibration curve is the function of T vs MO when no obstacle intervenes between the sensor and the target. The monopulse processor output is determined by three items: the field at the antenna surface, the gain illumination pattern of the antenna, and the monopulse processing scheme. A description of these three items follows.

The field at the surface of the antenna, with its boresight pointed at the aircraft, is determined by the dimension of the obstacle and its position with respect to the sensor. Assume the obstacle is a tall opaque mask with a cross-range width of OW (λ), R (λ) away from the sensor, and its center is at angle OA (degrees, clockwise) with respect to the target bearing. Normalizing the free space downlink field at the sensor antenna to unity, the field at the antenna after diffraction by the smokestack is FA_0 [Ref. 3]:

$$FA_0(X) = \frac{1}{\sqrt{2j}}\left[1 - (c(\alpha_2) - c(\alpha_1))\right]$$

$$+ j\left[1 - (S(\alpha_2) - S(\alpha_1))\right]$$

$$\alpha_1 = \sqrt{2}\left[\frac{R/\lambda * \tan OA/\lambda + \frac{OW}{2\lambda} - X/\lambda}{\sqrt{R/\lambda}}\right]$$

$$\alpha_2 = \sqrt{2}\left[\frac{R/\lambda * \tan OA/\lambda - \frac{OW}{2\lambda} - X/\lambda}{\sqrt{R/\lambda}}\right] \qquad (A.1)$$

where C and S are the Fresnel integrals, and X (λ) is the distance from the center of the antenna along its surface (see Figs. A-1 and A-2 for examples).

If the antenna is rotated so that the target is at an angle T (degrees clockwise) with respect to antenna boresight, a path difference (phase component) is introduced to FA_0, the field at the surface is FA

$$FA(X) = FA_0(X) * e^{J2\pi * X * \sin T/\lambda} \quad . \qquad (A.2)$$

The illumination pattern for the antenna horizontal distribution network is given in Table A-1. $G\Delta_i$ denotes the difference pattern, and $G\Sigma_i$ the sum pattern. The spacing between the columns elements is 8.36 inches corresponding to 8.36/12 λ. The antenna sum and difference channel outputs, Δ and Σ, are given by

$$\Delta = j \Sigma FA(X_i) G \Delta_i$$

$$\Sigma = \Sigma FA(X_i) G \Sigma_i \qquad (A.3)$$

where X_i is the position of element i with respect to the antenna center.

The monopulse processor output, MO, is based on a description given by Sussman [Ref. 2].

$$MO = [\arg (\Sigma + j \Delta) - \arg (\Sigma - j \Delta)] \qquad (A.4)$$

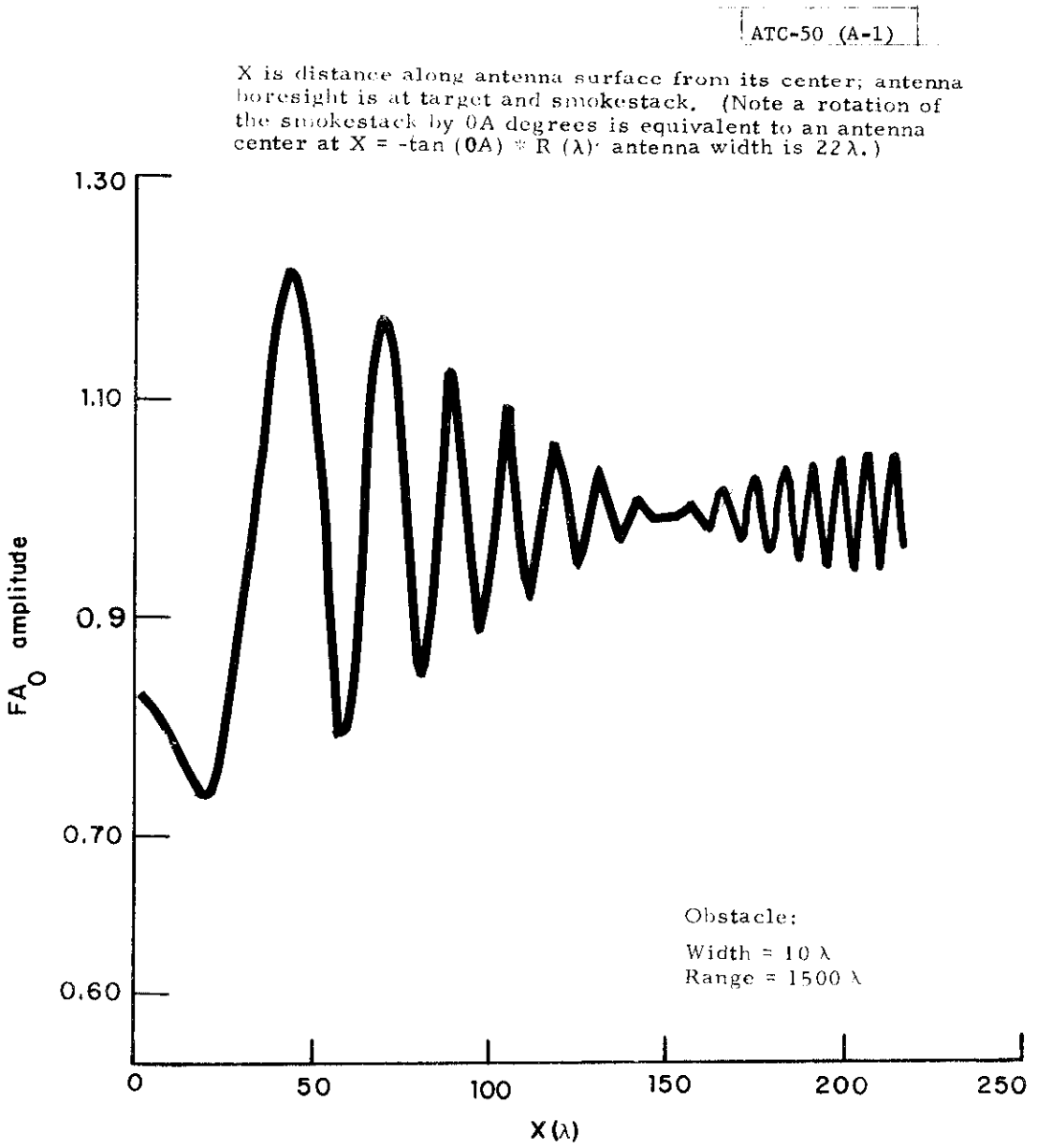

Fig. A-1. Amplitude of the field after diffraction (FA_o) at the antenna surface.

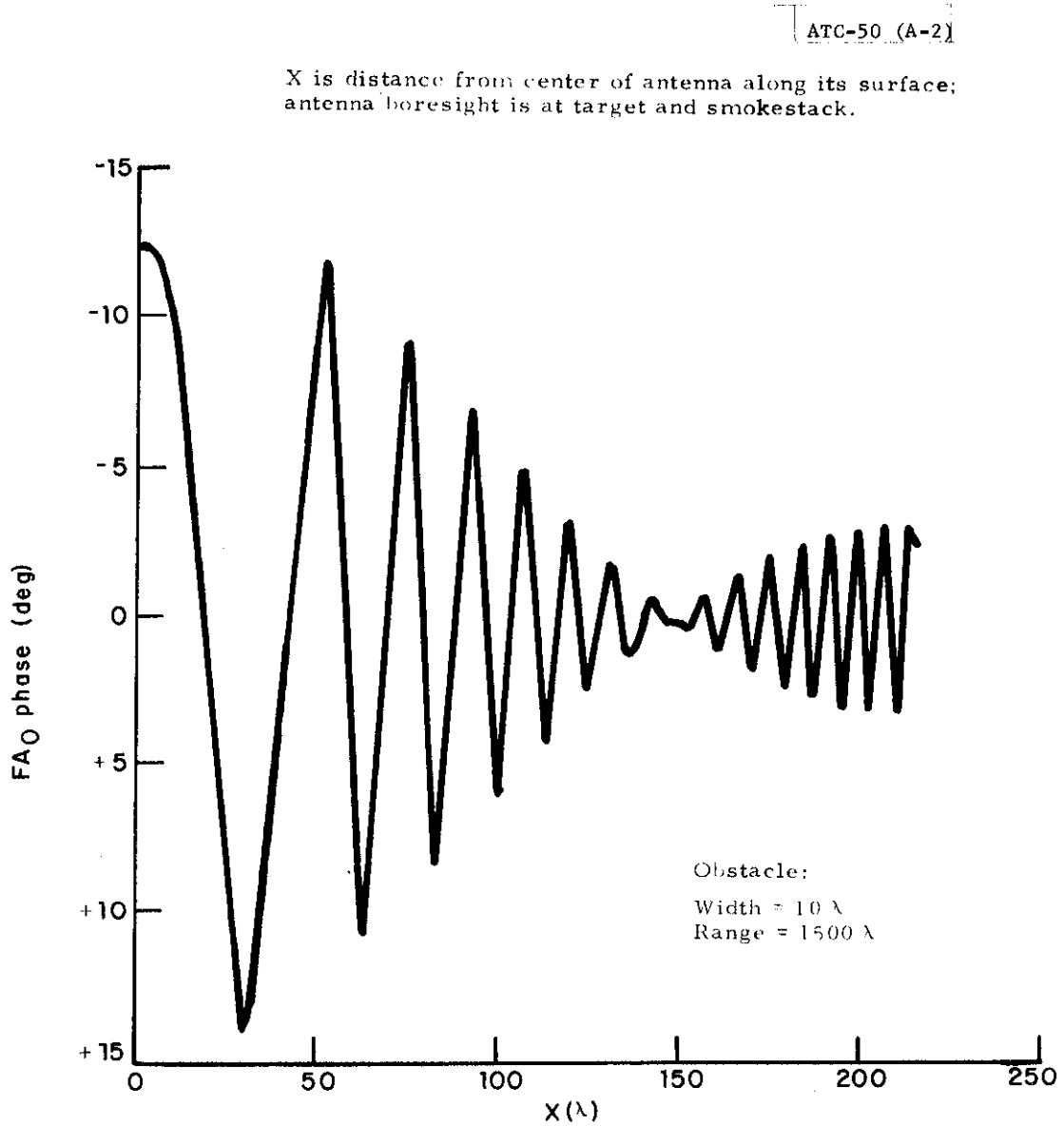

Fig. A-2. Phase of the field after diffraction (FA_o) at the antenna surface.

TABLE A-1. RELATIVE DRIVING VOLTAGE[3] AMPLITUDE DISTRIBUTIONS FOR THE SUM AND DIFFERENCE PATTERNS OF DABSEF.

(Columns are numbered from the center of the array.)

Column No.	$G\Delta$	$G\Sigma$
1	0.110	0.913
2	0.324	0.898
3	0.515	0.870
4	0.673	0.829
5	0.789	0.772
6	0.857	0.708
7	0.877	0.637
8	0.852	0.565
9	0.789	0.487
10	0.697	0.412
11	0.588	0.340
12	0.471	0.271
13	0.356	0.207
14	0.252	0.155
15	0.167	0.120
16	0.124	0.102

A.2 Sliding Window Azimuth Error

The sliding angle estimate is based on azimuth splitting the sum beam channel output; the target position is given by

$$1/2\left[\begin{array}{l}\text{Azimuth} \\ \text{of leading} \\ \text{edge}\end{array} + \begin{array}{l}\text{Azimuth} \\ \text{of trailing} \\ \text{edge}\end{array}\right]$$

where azimuth of leading (trailing) edge is the boresight azimuth, as the antenna sweeps by the aircraft, where the sum channel first (last) attains a power within THR (dB) from the peak power received on the sum channel (see Fig. A-3).

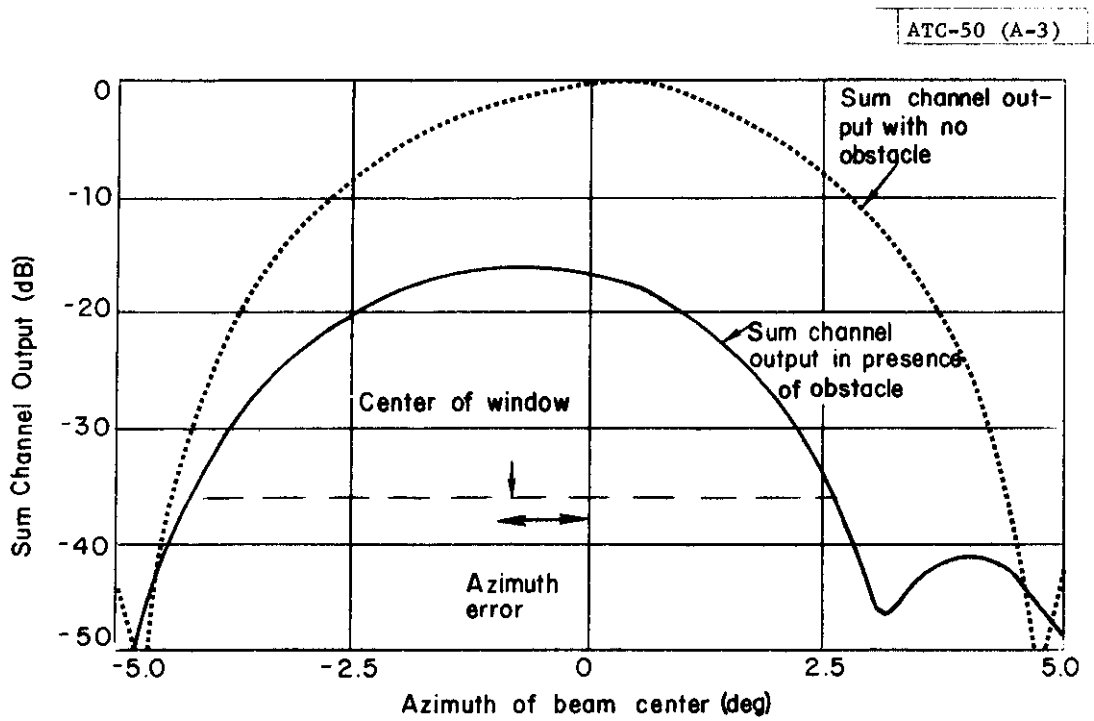

Fig. A-3. Effect of shadow of Prudential building on sum channel output.

APPENDIX B

SHADOW CAST BY OBSTACLES FOR AIRCRAFT AT CLOSE RANGE

In Appendix A, the method for computing azimuth error is discussed for an aircraft at long range from the sensor. When the aircraft is at close range, i.e., RA(λ), the range of the aircraft is comparable to the range of obstacle, R. Then in equation A.1 from [Ref. 3], the values of α_1 and α_2 become

$$\alpha_1 = \sqrt{2}\left[\frac{R}{\lambda} * \tan OA + \frac{OW}{2\lambda} - \frac{x}{\lambda}\right] / \sqrt{Re/\lambda}$$

$$\alpha_2 = \sqrt{2}\left[\frac{R}{\lambda} * \tan OA - \frac{OW}{2\lambda} - \frac{x}{\lambda}\right] / \sqrt{Re/\lambda} \qquad \text{(B. 1)}$$

where

$$Re = \frac{Rx[RA - R]}{RA}$$

and

$$Ra > R \quad .$$

Consider the normalized shadow strength, FSHADOW cast by the obstacle with respect to the downlink field strength, then

$$FSHADOW = 1 - FA(x)$$

$$= \frac{1}{\sqrt{2j}}\left[c(\alpha_2) - c(\alpha_1) + j(s(\alpha_2) - s(\alpha_1))\right] . \qquad \text{(B. 2)}$$

If the obstacle width << R_e, a situation corresponding to a weak obstacle shadow, then

$$|\text{FSHADOW}| \approx \text{CONSTANT} * \frac{OW}{\lambda\sqrt{R_e/\lambda}} \quad . \qquad \text{(B. 3)}$$

Combining equations B. 1 and B. 3 and considering the obstacle shadow a function of its range, we have

$$|\text{FSHADOW}| \sim \sqrt{\frac{RA * \lambda}{R * (RA - R)}} \qquad \text{(B. 4)}$$

Equation B. 4 implies:

(1) Aircraft at close range (RA close to R) experience a larger azimuth error than at long range because the obstacle casts a stronger shadow.

(2) For a particular obstacle, aircraft with a range greater than 10 times that of the obstacle have the same azimuth error because

$$|\text{FSHADOW}| \sim \sqrt{\frac{\lambda}{R}}$$

APPENDIX C

METHOD OF COMPUTING MONOPULSE AZIMUTH ERROR FOR A REFLECTING DISH ANTENNA

In Appendix A, the antenna was assumed to be a planar array. The method of computation is readily adpated to a reflected dish antenna. The equivalent illumination pattern for the reflecting dish is obtained from the receive azimuth pattern of the feed and the position of the feed with respect to the reflector. Figure C-1 shows the received sum and difference feed patterns for the Modified ASR-7 antenna, which is a 17.5-ft wide reflecting dish antenna (17.5 λ at DABS frequency) [Ref. 4]. The feed is 58 inches away from the surface of the antenna. The antenna illumination is represented by a planar array with 32 elements, equally spaced across the surface, for each of the sum and difference patterns. The gain of the element (sum or difference) is obtained from Fig. C-1. The azimuth of the element with respect to the feed, AZF, is given by

$$AZF = \tan^{-1}\left[\frac{\text{distance of element from antenna center}}{\text{distance of feed from antenna surface}}\right].$$

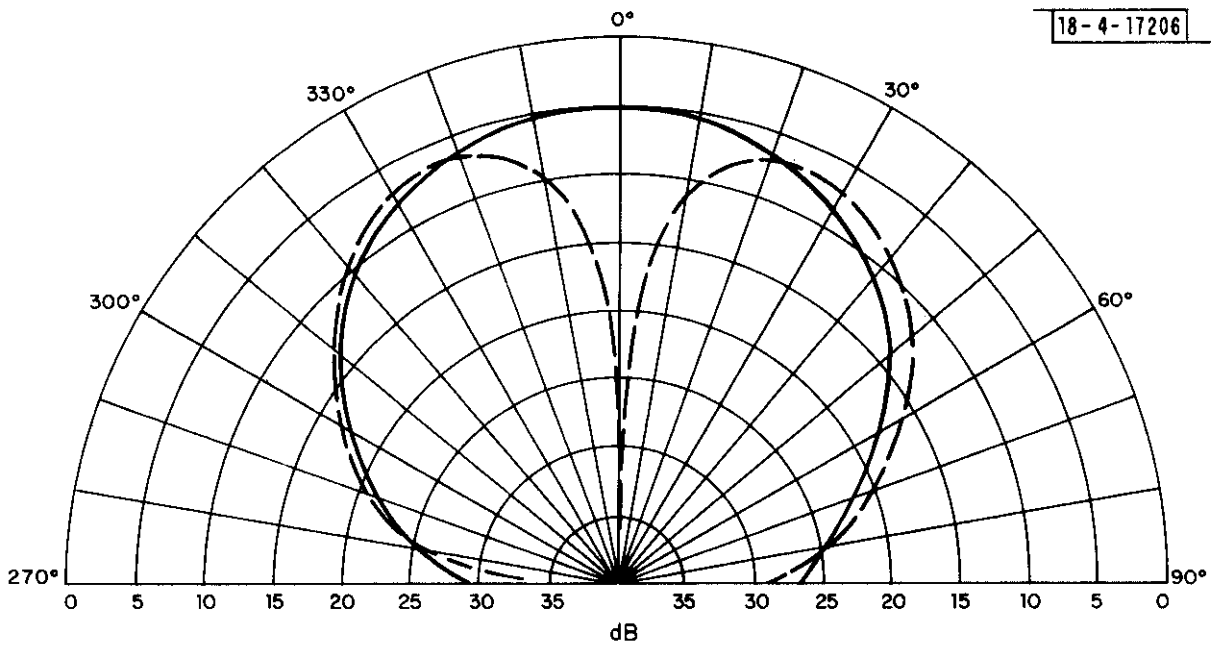

Fig. C-1. Receive sum and difference feed patterns in azimuth.

REFERENCES

[1] P. R. Drouilhet, "DABS: A System Description," Project Report ATC-42, Lincoln Laboratory, M. I. T. (18 November 1974), DDC AD-A005056/7.

[2] "Development of a Discrete Address Beacon System," Quarterly Technical Summary, Lincoln Laboratory, M. I. T. (1 October 1974), Figs. VIII-12 to VIII-14, DDC AD-A002399/4.

[3] A. Spiridon, "Effects of Local Terrain and Obstacles Upon Near Horizon Gain of L-Band Beacon Antennas," Technical Note 1975-6, Lincoln Laboratory, M. I. T. (17 July 1975).

[4] "Discrete Address Beacon System (DABS) Feed Modification for the ASR-7 Radar Antenna," Texas Instruments, Inc. (25 January 1974).